THESIS FOR THE DEGREE OF LICENTIATE OF ENGINEERING

Deformation behaviour of A356 - T7 cast aluminium alloys used in high specific power IC engine cylinder heads

Elanghovan Natesan

CHALMERS

Department of Industrial and Materials Science
CHALMERS UNIVERSITY OF TECHNOLOGY
Gothenburg, Sweden, 2019

Deformation behaviour of A356-T7 cast aluminium alloys used in high specific power IC engine cylinder heads

Elanghovan Natesan

No. IMS-2019-3

Department of Industrial and Materials Science
Chalmers University of Technology
SE-412 96 Gothenburg
Sweden
Tel: +46 (0)31 772 1000

Printed by Chalmers Reproservice
Gothenburg, Sweden 2019

Deformation behaviour of A356-T7 cast aluminium alloys used in high specific power IC engine cylinder heads

Elanghovan Natesan
Department of Industrial and Materials Science
Chalmers University of Technology

Abstract

The constant development drive towards higher specific power and lower displacement engines in recent years to produce environmentally friendly high-performance cars has placed increasingly high thermal loads on the internal combustion engine materials. Further, the advent of hybrid power trains placing higher demands on quick starts and a rapid approach to maximum power necessitates the automotive industry to move towards a more robust computational thermo-mechanical fatigue life prediction methodology to develop reliable engines and reduce developmental costs. The overarching goal of the research project is to develop constitutive and lifetime prediction models with just the necessary and sufficient parameters to predict the thermo-mechanical fatigue life of the highly loaded engine cylinder heads. The cylinder heads of the internal combustion engines are often made with primary A356 cast aluminium alloys and are employed in a T7 overaged condition.

The present thesis aims at establishing the mechanical deformation and fracture behaviour of the material with test samples extracted from the highly loaded valve bridge regions of specially cast cylinder heads made of the said A356 - T7 alloy. The deformation behaviour of the alloy is predominantly determined by the cast microstructure characterized by the dendritic arm spacing, the size of the secondary precipitates, the various defect distribution and by the temperature during deformation. The scope of this study covers uniaxial isothermal tests to establish the cyclic deformation behaviour and fatigue properties of the alloy at temperatures ranging from the ambient temperature to 250 °C. Completely reversed strain controlled uniaxial low cycle fatigue tests are run at three different total strain amplitude levels of 0.2, 0.3 and 0.4 % with multiple replicas at a constant strain rate of 1 % sec^{-1} to capture the cyclic deformation behaviour and the corresponding temperature dependent fatigue life curves. The model parameters of a suitable constitutive model are calibrated to predict the non-linear stress-strain response under thermal and mechanical load cycling. Monotonic deformation tests are also performed at the standard strain rate of 0.01 % sec^{-1} at varying temperatures from the ambient to 300 °C to establish the base material mechanical properties.

The material has an elastic-plastic monotonic response with significant hardening exhibited at temperatures around and lower than 150 °C and softening with plastic deformation at temperatures above 150 °C. The strength of the material decreases with increasing temperatures with corresponding increase in ductility. The material exhibits cyclic hardening at room temperature and cyclic softening at and above 150 °C in strain controlled completely reversed cyclic tests. The material exhibits decreasing peak stress response and increased plastic strain amplitudes with increasing temperatures in cyclic loading. The experimental data is calibrated against the Chaboche model with multiple back stresses to capture the temperature dependent kinematic and isotropic hardening behaviour of the alloy. The material exhibits a non-linear deformation behaviour with a mixed isotropic and kinematic hardening behaviour that can be modelled using a linear and a nonlinear backstress. The material exhibits significant scatter in measured mechanical properties at lower temperatures between replicas owing to the diverse microstructure obtained owing to material variability between the extracted samples. Increase in test temperatures shows a reduction in the said scatter indicating a waning influence of the microstructure on the deformation behaviour at elevated temperatures. A dilatometric study of the material using a cylindrical specimen indicates a stable coefficient of thermal expansion in the temperature range of 25 – 250 °C.

Keywords: cylinder head, fatigue, constitutive models, thermo-mechanical fatigue

Preface

This work was carried out at the Department of Industrial and Materials Science, Chalmers University of Technology, Gothenburg, Sweden between September 2016 and December 2018 under the supervision of Professor Christer Persson and Professor Johan Ahlström. The research was financially supported by FFI and Volvo Cars under the project 'Utveckling av Analysmodeller för Termomekanisk Utmattning' planned between October 2013 and May 2019. This licentiate thesis comprises of testing and modelling of the time independent plastic deformation and fatigue behaviour of A356-T7 cast aluminium alloys extracted from highly loaded valve bridges of specially cast cylinder heads at various temperatures.

List of appended papers

I. **Deformation and Fatigue Behaviour of A356 - T7 Cast Aluminium Alloys Part I: Room Temperature**
E. Natesan, C. Persson, J. Ahlström
Manuscript, partly presented at 11th International Conference on Advanced Computational Engineering and Experimenting (ACEX2017), Vienna, Austria

II. **Deformation and Fatigue Behaviour of A356 - T7 Cast Aluminium Alloys Part II: Elevated Temperatures**
E. Natesan, M. Vogler, C. Persson, J. Ahlström
Manuscript, partly presented at 12th International Fatigue Congress 2018, Poitiers, France

Contribution to the appended papers

I. The author planned and performed the experimental and modelling work and wrote the paper in cooperation with the co-authors.

II. The author planned and performed the majority of the experimental and modelling work and wrote the paper in cooperation with the co-authors.
Ageing studies were performed by Monika Vogler, University of Stuttgart, Germany.
Dilatometric tests were performed by Lic. Eng. Johan Wendel, Chalmers University, Sweden.

Contents

1. Introduction 1
1.1 Background 1
1.2 Challenges in Complete Electrification & Hybrid Technology 1
1.3 Aim of the Study 2
2. Thermo-Mechanical Fatigue 3
2.1 Fatigue: An Introduction 3
2.2 Thermo-Mechanical Fatigue in Cylinder Heads 3
3. Material: Cast Aluminium Alloys 7
3.1 Aluminium Alloys: An Introduction 7
3.2 Material for Testing 9
3.3 Test Methods and Apparatus 11
4. Results and Summary of Appended Papers 17
4.1 General Observations 17
4.2 Monotonic Deformation 17
4.3 Cyclic Deformation 19
4.4 Dilatometry 32
5. Conclusions 33
6. Future Work 35
7. Acknowledgements 37
8. References 39

1. Introduction

1.1 Background

“Modern technology has become a total phenomenon for civilization, the defining force of a new social order in which efficiency is no longer an option but a necessity imposed on all human activity” said the famous French philosopher Jacques Ellul. The industries of the world have constantly strived to increase their energy efficiency and move towards renewable and more sustainable sources of power with the glaring exception of the transportation industry over the last few decades [1].

Mechanical power trains with more than 150 year old internal combustion engines have remained largely inefficient with average efficiencies of about 20 % [2]. With the ever tightening environmental regulations to improve the quality of ambient air with a focus on urban air quality in particular, auto manufacturers have been increasingly looking at electrification of the vehicle power trains to meet the emission norms [3]–[5]. While the concept of electric or electrified powertrains have been around for well over a century [6]–[8], the advent of electric powered means of private transportation has been hindered primarily by the prohibitively expensive prices, the size and capacity of the traditional batteries coupled with long charging durations and several other practical challenges [1], [7]. Remarkably, electric cars were a third of all road vehicles sold around the 1900s in the USA [7] at a time when the society was gradually moving away from horse drawn carriages with steam powered, electric and internal combustion engine cars getting increasingly popular. While the steam powered cars were notoriously difficult to operate, the internal combustion engine cars with their manual cranks, difficult to operate gear system and noxious fumes were not too popular either. Electric cars were getting increasingly prevalent owing to their ease of use and practicality before the introduction of the first mass produced internal combustion engine car, the Ford Model T that made personal vehicles accessible to the general public with its significantly lower cost. Coupled with the introduction of the electric starter motor by Charles Kettering obviating the need for hand cranks in ICE cars and the cheaper and more easily accessible petroleum fuel products in comparison to electricity that was only available in the cities, there was a gradual decline in interest in electric powered cars until they virtually became non-existent by 1935 [7]. While there was a brief resuscitation of interest in the electric and hybrid technology during the 1973 oil crisis [9], the eventual stabilization of the oil prices and the underperformance, limited range and still prohibitive cost of manufacturing electric vehicles ensured that the idea of electrified powertrains never took off [7]. Continuing technological advances in the battery technology primarily driven by the consumer electronic industry, and especially those that of the lithium ion chemistry and solid state batteries, has been leading to a gain in traction of battery electric vehicles in recent years [10], [11] both of these arenas will only improve the outlook for hybrids and electric vehicles.

1.2 Challenges in Complete Electrification & Hybrid Technology

The primary challenges in complete electrification is the cost of the batteries and consequently, the car, range anxiety, need of specialized charging stations to have quicker recharge time, the cost and sustainable mining of the rare earth elements used in the batteries, battery recycling and not least of all, the inability to constantly extract good performance from the electric powertrain without causing battery overheat issues.

Hybrids offer a desirable balance owing to their high performance, lower cost of operation and the ability to run with petroleum fuel thus mitigating the range anxiety that has proved to be one of the biggest obstacles in complete electrification of our vehicles. With increasing oil prices, governments worldwide are offering subsidies and policy changes to help adopt electrified vehicles faster. Unlike conventional combustion engine cars, performance doesn’t

come at the cost of fuel efficiency and air pollution in hybrid vehicles. They offer a more practical solution to the transportation problem compared to bio-fuel and hydrogen powered vehicles. While the future will in all probability be electric, hybrids offer a perfect balance between the worlds old and new. As part of the new adoption of wide scale hybrid powertrains, automakers are continually looking at engine downsizing and induction charging techniques to reduce the weight and increase efficiency and performance simultaneously.

1.3 Aim of the Study

This constant drive towards higher specific power and lower displacement engines in recent years place increasingly higher thermal loads on the internal combustion engine materials. Further, the advent of hybrid power trains placing higher demands on quick starts and a rapid approach to maximum power necessitates the automotive industry to move towards a more robust computational thermo-mechanical fatigue life prediction methodology to develop reliable engines and reduce developmental costs. The study aims to develop constitutive and lifetime prediction models with just the necessary and sufficient parameters to predict the thermo-mechanical fatigue life of the highly loaded engine cylinder head.

2. Thermo-Mechanical Fatigue

2.1 Fatigue: An Introduction

Repeated loading of engineering structures, even at load levels much lower than a material's strength, can lead to microstructural damage initiation and accumulation leading to fatigue failures. An estimated 80 % of all structural failures have some contribution from fatigue related damage, its cost, amongst industrialized nations, estimated at about 3 % of their GDP [12]. Owing to engineering efforts in the last 150 years, fatigue is a well explored subject with broadly three different approaches adopted for designing structures against fatigue failure [12], namely:

- stress based approach that uses the nominal stress in the region of interest,
- strain based approach that takes a more detailed look at localized plasticity,
- fracture mechanics approach that explicitly deals with the growth of cracks.

The development of numerical simulations and the incredible leaps made in computing technology in the last decades have enabled engineers to compute structural responses and predict component life in increasingly shorter times.

2.2 Thermo-Mechanical Fatigue in Cylinder Heads

A cylinder head is part of an internal combustion engine and sits on top of the engine cylinder block. It serves as the upper deck of the combustion chamber and houses the cam shaft, inlet and exhaust valves, cooling channels and other assorted components. It also serves as a passage way for the inlet and exhaust gases and consequently has huge thermal gradients and with engine cooling, different parts of the cylinder head experience different temperature cycles during a typical operation.

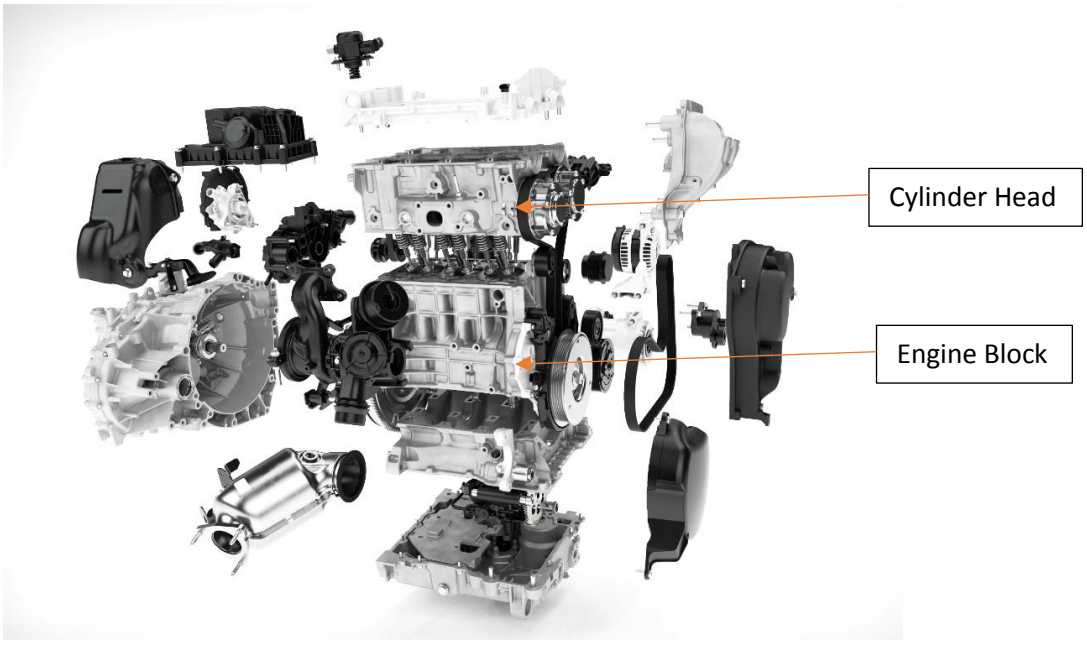

Figure 1: Internal combustion engine architecture [Source: Volvo Cars]

Besides the thermal loads associated with the combustion processes and the stresses in the material owing to steep thermal gradients, a cylinder head material should also support the mechanical assembly loads from bolts, gaskets, and operational mechanical loads from the valve operations that load the cylinder head through the valve seats [13]. Consequently, the cylinder head undergoes high cycle fatigue (HCF) associated with the combustion cycles at a

loading frequency corresponding to the engine rotational speed [14] and low cycle fatigue (LCF) associated with the engine start - stop cycle that is a combination of the thermal and mechanical loads resulting in thermo-mechanical fatigue failures (TMF) [13], [15], [16]. Physical TMF testing of cylinder heads is an expensive routine and so, development of a reliable simulation model is desirable to reduce developmental times and associated testing costs. During a typical TMF load cycle, the temperature of different parts of the structure varies from ambient to several hundred degree Celsius and since the material's mechanical behaviour varies with temperature, it is imperative to create temperature dependent constitutive and fracture models from the ambient to the maximum temperatures in the structure expected during operation to get reliable simulation results [16]–[18]. To model the mechanical behaviour of the structure, one tactic is to take a physical approach that relates to the microscopic phenomena and that which is intricate and computationally expensive on an industrial context [17]. This study instead uses the other popular technique of macroscopic phenomenological approach that is a much faster and computationally inexpensive method.

As there is significant plastic deformation during the thermo-mechanical loading of the structure, a strain-life approach is often taken to model and predict the fatigue life of the cylinder heads [12], [16]. Since the strain based approach could also be used for long lives with mostly elastic deformation, it is a wide-ranging methodology [12] and is the topic of interest in this study. The strain-based approach to predict the fatigue life employs the strain life Coffin-Manson type model. It is especially suitable for applications that involve cyclic loading associated with thermal stresses and strains [12].

2.2.1 Modelling and Life Prediction

Thermo-mechanical life prediction by Thomas et al. [19] involved a comprehensive approach starting with thermal analysis to obtain the load history which was then combined with an elasto-viscoplastic mechanical analysis to predict the structural response. This was then used to predict the crack initiation points by using a suitable damage criterion coupled with fatigue life models. The prediction of the cylinder head life under thermo-mechanical loads is vital before the commencement of the mass production process. The temperatures in the cylinder head can vary from the environmental temperature in cold climates to 300 °C in highly loaded areas. To make things complicated, literature and internal studies have shown that the material exhibits an ageing behaviour at temperatures above 150 °C [19], [20]. Often times in modelling, a stabilized response of the material is assumed. But with ageing, studies have shown the effect on the life curves for instance [21], [22] and this muddles the process even further. To keep the simulations at a complexity level that is suitable in an industrial context, certain simplifications need to be made in the simulation process to obtain workable results [19].

A thermo-mechanical fatigue life prediction simulation can be briefly condensed to the following steps according to Thomas et al. [19]:

- Choosing appropriate cyclic viscoplastic model and calibration of the model parameters using isothermal and non-isothermal tests.
- Modelling of the ageing behaviour of the alloy.
- Choosing a suitable fatigue criterion based off isothermal and non-isothermal uniaxial tests with suitable loading conditions.
- Finite element simulation of the structure or sub-structure with realistic load and boundary conditions. The accuracy of the prediction is heavily influenced by the load and boundary conditions used when the constitutive and fatigue models are suitably calibrated.
- Use the chosen damage and fatigue criterion to analyse the structural response and determine the thermo-mechanical fatigue life of the component.

While in real life these scenarios play out simultaneously, to reduce the complexity of the simulation process, a decoupled approach is often suggested and have shown to give satisfactory results [16], [19], [23]–[25]. So, the thermal analysis and the mechanical analysis are handled separately and in the structural simulations, a further decoupling is assumed between the various phenomena, for example, the ageing evolution and the mechanical behaviour, the constitutive behaviour and the fatigue life modelling.

2.2.1.1 Constitutive Modelling

Since the thermal fatigue in the cylinder heads is fundamentally associated with the thermal loading associated with the engine start-stop, it is imperative to model the behaviour at elevated temperatures where the flow stresses are significantly lower than at room temperature. Dwell times enhance time dependent relaxation of the material and the cyclical nature of the thermal loads lead to high stresses and plasticity in confined regions like the exhaust valve bridges. This necessitates a visco-plastic model that is temperature dependent. To simplify the simulations, the visco-plastic model needn't include damage accumulation as several previous studies [19], [26] have showed that such a coupling is often unnecessary and often leads to difficulties in parameter calibrations and lengthy calculations without any improvement in the life estimations. The calibration can often be done on steady state cycles and the constitutive law should be robust enough to allow large time step integrations [19].

2.2.1.2 Fracture Modelling

The failure criteria in a thermo-mechanical context should be capable of predicting the failure in applications with transient operating temperatures and isothermal loads under uniaxial and multi-axial load conditions [27]. Once the mechanical response of the structure has been determined using the load history, the natural ensuing step in the design cycle is to determine the life of the component using a pertinent fatigue life criterion. While the constitutive behaviour could be coupled with the material damage in the material model, it is unnecessarily complex without any improved life prediction. Hence, a decoupled constitutive behaviour and fatigue life modelling is often adopted in the industry.

Due to the multiaxial and anisothermal nature of the real life structural loads in a thermo-mechanical fatigue context, there is a constant discussion over the suitability of multiple different techniques that can be used to predict the life of the components once the stress and strain history of the geometry is known. Coffin-Manson parametric models based off the plastic strain amplitude ($\Delta\varepsilon_{pa}$) have historically been used for fatigue life determination in the low cycle fatigue regimen. To account for mean strain and stress effects the Smith-Watson-Topper [28] and the popular Ostergren fatigue criterion use the maximum tensile stress in the fatigue criteria. These laws are empirical in nature and works well for most engineering metals but don't have physical meaning in terms of deformation and fracture. Generalization of these classical laws for multi-axial and anisothermal loads can often be tedious because of the varying yield in isothermal conditions and with them not being intrinsic in general [25].

To tackle such issues, Morrow et al. [29], [30], Benham et al. [31] pioneered the use of an energetic criteria for determining the fatigue lives of engineering metals. Broadly speaking they propose quantitative relations between the plastic strain energy (per cycle or the total plastic strain energy) to the fatigue life of metals with the assumption that the plastic strain energy in cyclic loading as a measure of the fatigue damage. Subsequently many researchers have studied the suitability of the energy criterion in a TMF context with varying temperatures and mechanical loads. Charkaluk et al. [19], [25] propose dissipated energy per cycle from the saturated state as a more suitable and better fatigue criterion for the multi-axial anisothermal loads in the cylinder head compared to the classical Coffin-Manson or Ostergren fatigue criteria. In order to account for strain rate effects in TMF, Takahashi et al. [18] propose using the dissipated energy rate per cycle as a suitable criterion for complex loads with different loading rates. Energetic approaches despite being deemed suitable for anisothermal and

complex multi-axial loads are often criticized for failing to distinguish between the dissipated heat energy in a load cycle and the portion contributing to damage [25].

3. Material: Cast Aluminium Alloys

3.1 Aluminium Alloys: An Introduction

Aluminium alloys are extensively used in structural components owing to their low density, good thermal and electrical conductivities, good corrosion resistance and a number of other desirable properties but are often limited in their use in high temperature applications owing to their low melting point [32]. The mechanical properties can be tailored with alloying and cold working, with most alloyed materials being capable of heat treatment with the precipitates often forming from elements not dissolved in the solid solution.

Aluminium alloys in their various forms are widely used in the aircraft, automotive, food and numerous other industries. Aluminium has especially gained traction in the automotive industry in recent years owing to its impressive specific material properties. Its low density and high mechanical performance leads to an improved performance on a per weight basis compared to traditional materials like steels enabling the vehicle manufacturers to drastically cut down the weight of their products and in turn improving the vehicle efficiency and lowering the environmental impact [32].

3.1.1 General Introduction & Classification

Aluminium alloys are broadly categorized as cast and wrought. The compositions and purity levels are often indicated with three or four digits indicating the principal alloying elements and the purity level of the alloy. The temper designation follows these numerals after a hyphen and is specified with a letter followed by various numbers indicating the various mechanical and heat-treatment that the material is subjected to. F, H and O are used to indicate as-fabricated, strain hardened and annealed states in that order [32] for example. A T7 temper designation indicates a solution treatment followed by artificial over-ageing of the material [32].

3.1.2 Aluminium Alloys in the Automotive Industry

Besides the chassis, aluminium alloys are widely used for producing various parts of the internal combustion engine like the engine blocks, cylinder heads, pistons, inlet and exhaust manifolds among many others.

Cylinder blocks and cylinder heads often owing to their complicated geometry are mass produced by casting processes. Different casting processes like sand casting, die casting, investment casting, lost foam casting, etc. are often used depending on the volume of production, quality of casts required, mechanical properties desired among other considerations [32].

3.1.3 Microstructure of A356 Alloys

The microstructure of the A356 family of alloys can be broadly classified down to three different components [33]:

1. primary α-Al solid solution phase,
2. Al-Si eutectic,
3. other intermetallics and secondary phases arising out of components not dissolved in the primary solid solution.

The size, volume, morphology and distribution of these microstructural features have a profound impact of the deformation behaviour of the alloy and are largely determined by the specific alloy composition, manufacturing methods, post-treatment and service conditions [33].

3.1.4 Role of Alloying Elements

Silicon

Owing to the eutectic formation in the binary Al - Si alloy, silicon is added in cast aluminium alloys to reduce the melting point of the alloy. It also has the added advantage of reducing the volumetric shrinkage of the structure during solidification [33]. The amount of silicon present in the alloy primarily determines the proportion of the Al-Si eutectic formed in the microstructure. Silicon addition also improves the wear properties and the dimensional stability of the structure. It further improves the strength and toughness of the alloy [34].

Copper

Copper addition typically promotes the formation of Cu rich intermetallics like the θ (Al_2Cu) that improve the high temperature strength of the alloy even though it comes at the cost of reduced ductility. Copper rich precipitates are more resistant to shearing by dislocations, thus providing increased hardening [35], [36]. Increasing the copper content also results in an increased volume fraction of porosity due to the increased solidification interval in the castings [33].

Magnesium

Age hardening behaviour is induced in Al - Si castings by the addition of magnesium as a vital alloying element. It forms Mg -Si precipitates that are highly effective in strengthening and can be heat treated to tailor the mechanical properties of the alloy [37], [38]. However, studies have indicated that the dimensional stability of the casting is affected by increased magnesium content [39].

Iron

Iron is treated as an impurity in the Al - Si cast alloys in general. Due to the low solubility of Fe in the aluminium alloys, it forms brittle intermetallic particles that tend to have a deleterious effect on the ductility of the material. Low magnesium content in the range 0.3 - 0.5 % aids marginal improvement in ductility by partially transforming the brittle iron containing intermetallics to fine scale β particles during the heat treatment [33]. Studies have shown the influence of such β precipitates in the formation of porosities [40]–[42].

Manganese

Manganese serves to mitigate the deleterious effect of iron in Al - Si castings. In the presence of Mn, iron forms an intermetallic α phase in place of the β platelets with the former improving the ductility of the material [33]. α phase also reduces the shrinkage porosity in the cast structure [43].

Other Alloying Elements

Sodium is often added to modify the microstructure and produce fine interconnected fibrous phase distribution in the eutectic structure [44], [45] that gives better toughness and ductility. Boron and titanium are added to refine the grain size of the cast structure by promoting the nucleation rate during solidification [44], [46]. Strontium is often added to the alloy to modify the Al-Si primary eutectic to a fine fibrous phase brought about by changes in nucleation and growth of the eutectic phase [45], [47].

3.1.5 A356 Cast Aluminium Alloy in Cylinder Heads

Cast aluminium alloys of the Al - 7 Si - Mg type like the A356 family of alloys are widely used for structural castings with complex geometries owing to their good castability, high strength, high toughness and a reduced tendency to form casting defects [33]. For applications like cylinder heads in the internal combustion engines where the ductility takes lower priority than the high temperature strength, copper is often added to varying degrees to improve the elevated temperature mechanical properties even if it comes at the cost of increased porosity and susceptibility to hot cracking [33].

3.1.6 Influence of Microstructural Features

A number of factors besides the chemical composition affect the mechanical deformation and fatigue behaviour of the A356 family of alloys [33]. Studies have shown the effect of the as-cast microstructure influenced by the chemical composition and cooling rates, the heat treatment that the structural material is subjected to and service temperatures on the mechanical behaviour of the material [37], [48]–[52]. The life of the A356 - T7 aluminium alloy cylinder heads is found to be often dictated by the casting defects and other microstructural features like the secondary dendrite arm spacing, the morphology and size of the secondary particles [53]. Studies on fracture surfaces by Fuoco et al. [54] on fatigue cracks in aluminium cylinder heads show cracks originating from micro-porosities and oxide film inclusions. Fatigue damage studies by Koutiri et al. [55], [56] on A356 - T7 alloys identified two competing fatigue damage mechanisms with the micro-shrinkage pores playing a very fundamental role in dictating the fatigue behaviour. In the absence of the micro-shrinkage pores, the fatigue behaviour was controlled by other microstructural inhomogeneities like the secondary precipitates that affect the crack initiation. In addition, they found no significant difference in the fatigue strength of the material under uniaxial and biaxial stress states in A356 + 0.5 % Cu - T7 group of alloys contrary to the prediction of most multi-axial fatigue criteria [55], [56].

3.2 Material for Testing

3.2.1 Material Chemistry and Microstructure

The material for testing was extracted from specially cast cylinder heads made of A356 + 0.5 % Cu cast aluminium alloys subjected to a T7 heat treatment. The average chemical composition of the alloy as determined using a modified ASTM E1251 [57] analysis of Al-base using optical emission spectrometry [58] on two specimens extracted from the cylinder head is as presented in Table 1. The microstructure of the alloy indicating the primary α-Aluminium phase, the Al-Si eutectic and the visible intermetallics of the Mg, Cu, Fe, Mn, etc., elements whose solubility exceed that of the α - Al phase are shown in Figure 2 (a) and (b). The material exhibits a dendritic microstructure with the primary aluminium skirted by the Al-Si eutectic interspersed with the intermetallics formed by elements exceeding the solubility limit in the primary aluminium.

The dendritic arm spacing, size, shape and morphology of the secondary phases are a function of the chemical composition, cooling rates and the heat treatment and it tends to vary over the geometry of the cylinder head. All the micrographs and other measurements presented in this work pertain to the highly loaded valve bridge area of the cylinder head which is expounded in the succeeding section detailing the specimen extraction zones. The secondary dendrite arm spacing determined using the mean linear intercept method on the aligned sets of the secondary cells was between 30-32 µm at the centre of the specimen and with about 5 % reduction closer to the mould walls where the associated cooling rates are higher.

Table 1: Chemical composition of A356 + 0.5 % Cu - T7 cast aluminium alloy as tested in wt. %

Si	Cu	Mg	Ti	Fe	Mn	B	Others	Al
6.8	0.53	0.35	0.12	0.10	0.07	0.0012	<0.05	Bal

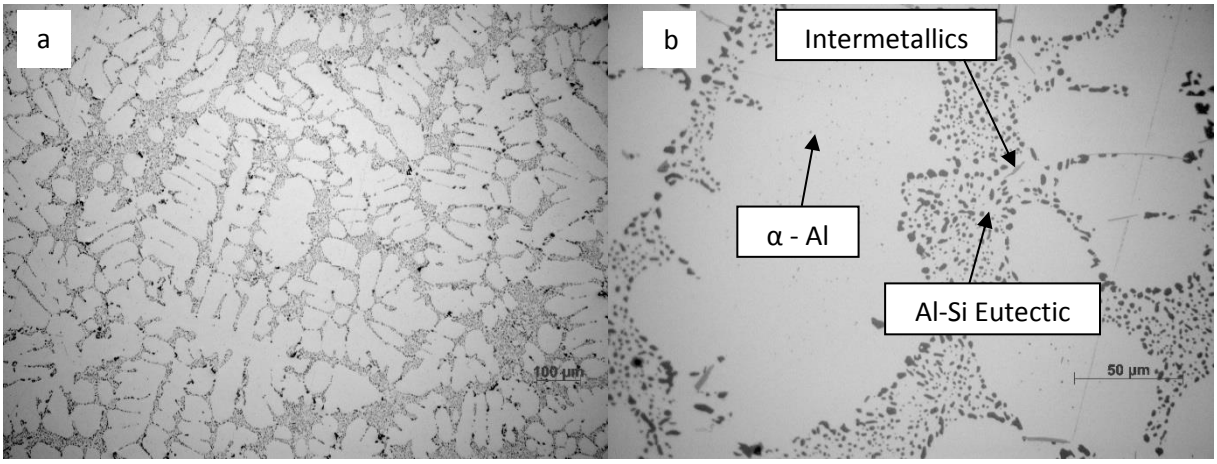

Figure 2: Representative optical micrograph from the tested A356-T7 alloy

3.2.2 Sample Extraction from Cylinder Heads

A cylinder head has a highly complex geometry with the material thickness differing from region to region. When such an intricate structure is cast, the cooling rate is different in different parts of the mould. As a result, the dendritic arm spacing and consequently, the deformation behaviour, damage mechanisms and the fatigue lives of the material varies through the geometry [27], [33] and is highly dependent upon where the test specimens are extracted from. It is of interest to study the deformation behaviour of the material that is critically loaded in the thermo-mechanical fatigue (TMF) context that which is the focus of the current research work. Numerous studies have shown that the material in the valve bridge areas experience the steepest thermal gradients during the engine start-stop cycle and tends to crack first [13], [53], [59] and hence is the region of interest in this study. Figure 3 shows the location of the extracted material that was used for establishing the deformation behaviour of the alloy. The test bars were carefully extracted, such that the test volume corresponded to the valve bridge area that was most sensitive to thermo-mechanical fatigue cracking. The extracted material was machined according to the ASTM test standard recommendations to the geometry as shown in Figure 4. While it is possible to cast test specimens, it often is difficult to replicate the complex microstructural variations often found in the cylinder heads produced by industrial manufacturing processes [55] and hence, the cast cylinders heads were used to extract the test specimens.

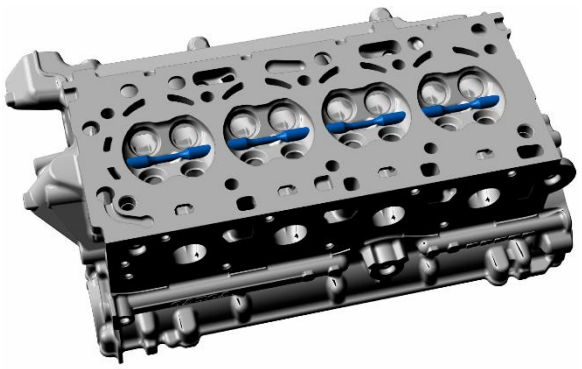

Figure 3: 3D CAD rendering indicating the specimen extraction zones

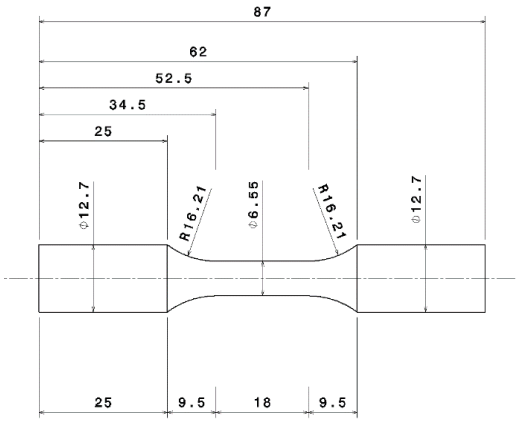

Figure 4: Test bar geometry machined in accordance with ASTM standards

3.3 Test Methods and Apparatus

3.3.1 Test Plan

The testing is aimed at establishing the uniaxial monotonic and cyclic deformation behaviour with an aim to model the constitutive and fatigue behaviour of the alloy at various temperatures of interest to aid in the thermo-mechanical fatigue life prediction.

Monotonic Deformation:

Monotonic tensile tests were performed to establish the base deformation behaviour of the material at room temperature, 100, 150, 200, 250 and 300 °C with a minimum of 2-3 tests at each temperature. The tests were performed using strain control according to the ASTM E8/E8M Tensile Testing guidelines [60] with a strain rate of 0.01 % sec^{-1}. All tests except at 300 °C were performed to fracture to obtain the ductility and toughness of the material at various temperatures. The tests at 300 °C exceeded the extensometer tensile strain limit of 18 % and the material stress response is presented till the threshold strain value tested.

Cyclic Deformation:

Strain Controlled Tests

Cyclic strain controlled low cycle fatigue tests were carried out in accordance with the ASTM E606/E606M standard for strain controlled fatigue tests [61] with different strain amplitudes at room temperature, 100, 150, 200, and 250 °C with a minimum of 2-3 tests at each load level to develop comprehensive strain-life curves that could even be used in situations where there is little plastic deformation and long lives are anticipated. The strain-controlled fatigue tests were performed with three different total strain amplitudes of 0.2, 0.3 and 0.4 % and a strain ratio of R_ε = - 1. The strain cycling followed a triangular wave format at a constant strain rate of 1 % sec^{-1} by using the corresponding loading frequencies. All samples were run to failure to develop the strain life curves at different temperatures. A sample is considered to have failed when the peak stress amplitudes developed during a cycle had dropped below 75 % of the peak stress amplitudes recorded in the 25th strain load cycle. The cast structures often have residual stresses from the quench process associated with the heat treatment and in addition will have mechanical assembly loads [14]. Since the operational loads are further superimposed on the prior loads, it is of interest to study the cyclic deformation behaviour of the material when subjected to asymmetrical loads. To study the effect of mean strain, strain-controlled tests were carried out with mean strains of 0.2 % and -0.2 % and with a strain amplitude of 0.4 % in both cases at the same strain rate of 1 % sec^{-1} similar to the prior strain-controlled tests.

Stress Controlled Tests

To study the equivalence of stress and strain-controlled fatigue tests, equivalent stress-controlled tests were run to study the hardening and fatigue behaviour of the alloy. The stresses recorded at half the life of the strain-controlled tests ($N_f/2$) were used as the basis of the stress-controlled tests. The samples were cycled between the minimum and maximum stresses obtained at $N_f/2$ of the strain-controlled tests. The tests were run at the same frequency as the corresponding strain-controlled tests and with a triangular load wave. Since the strains developed during the stress-controlled tests had a small deviation from the strain amplitudes in the corresponding strain-controlled tests, we have a small variation from the strain rate of 1 % sec^{-1} used in the equivalent strain-controlled tests but their effect on the resulting mechanical properties are expected to be trivial.

Dilatometry

A dilatometric study was carried out using a cylindrical specimen with 10 mm diameter and 50 mm length in a horizontal pushrod NETZSCH DIL402C dilatometer to determine the coefficient of thermal expansion of the material at different temperatures. The A356 + 0.5 % Cu - T7 sample was subjected to a controlled temperature program in a nitrogen atmosphere with the temperature of the sample being raised from 25 °C to 360 °C with a heating rate of 1 °C min^{-1}. A contact pressure of 30 cN was exerted on the sample.

3.3.2 Sample Preparation

All test specimens were polished sequentially using the 500, 800, 1200, 2000 and 4000 grit SiC papers. Fine polishing was carried out using a diamond suspension with 3 µm particles and oxide polishing was carried out using a colloidal silica suspension with 0.04 µm particles. The ground and polished samples had a mirror surface finish with a resultant surface roughness of ca $R_a = 2$.

3.3.3 Test Apparatus

All tests were performed using an Instron 8501 servo-hydraulic testing machine equipped with a fast electronic control system and 1 kHz data logging system. All the elevated temperature mechanical tests were performed using the Instron 3119-407 series temperature chamber. The temperatures were monitored and controlled using the built-in K-type thermocouple and a Eurotherm 2408 controller. Two types of extensometers were used for measuring the strain, the tests at and below 150 ˚C were performed using the Instron 2620-603 axial clip on dynamic extensometer [62] and the tests above 150 ˚C were performed using the Epsilon 3555-010M-020 high temperature axial capacitive extensometer.

Figure 5: Instron 8501 Servo-hydraulic testing machine

Test Equipment: Instron 8501 Servo-Hydraulic Testing Machine

Specifications:

Max load: 100 kN
Feedback: LVDT, Load Cell or Additional extensometer
Instron 3119-407 Series Temperature Chamber for elevated isothermal mechanical tests
Grips: Instron fatigue rated mechanical grips

Test Equipment: Instron 3119-407-222 Environmental Chamber

Specifications:

Temperature Range: -150 ˚C to 350 ˚C
Heating: Forced convection using air
Eurotherm 2408 controller with K-type thermocouples in the temperature Chamber
Overall System Accuracy in the temperature range RT-300 ˚C: ±3.5 ˚C

Instron dynamic extensometer 2620-603

Type: Axial clip on dynamic extensometer with T1351-1007 knife edge

Model: 2620-603 | Dynamic Extensometer

Dynamic Extensometer for direct strain measurement and closed loop strain control. Suitable for tensile, compressive & fatigue testing, the extensometer has a 10 mm gauge length with a travel of ±1 mm giving ±10 % strain.

Frequency Response: 100 Hz

Temperature range: - 80 ˚C to + 200 ˚C

Epsilon high temp. axial extensometer
Model: 3555-010M-020 (Capacitive)

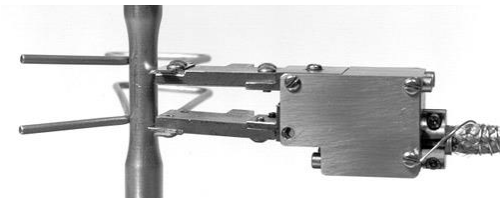

Type: Axial clip on capacitive extensometer with hardened tool steel knife edges

Model: 3555-010M-020 | High Temperature Axial Capacitive Extensometer

Dynamic Extensometer for direct strain measurement and closed loop strain control. Suitable for tensile, compressive & fatigue testing, the extensometer has a 10 mm gauge length with a travel of + 2 mm and - 1 mm giving a + 20 % and - 10 % strain range.

Frequency Response: Not Specified

Temperature range: Ambient to 540 ˚C

3.3.4 Heatup and Temperature Stabilization:

The heat up procedure is carried out under load control with no force exerted on the sample as the specimen and the equipment expanded with increasing temperatures. The overall quoted system temperature accuracy for the temperature range tested is ± 3.5 ˚C. The total heat up time and the time to reach the stable temperature condition accounting for equipment and sample expansion is about 3 hours. Figure 6 below shows the thermal expansion of the equipment (displacement) with time as the force on the sample is held at zero.

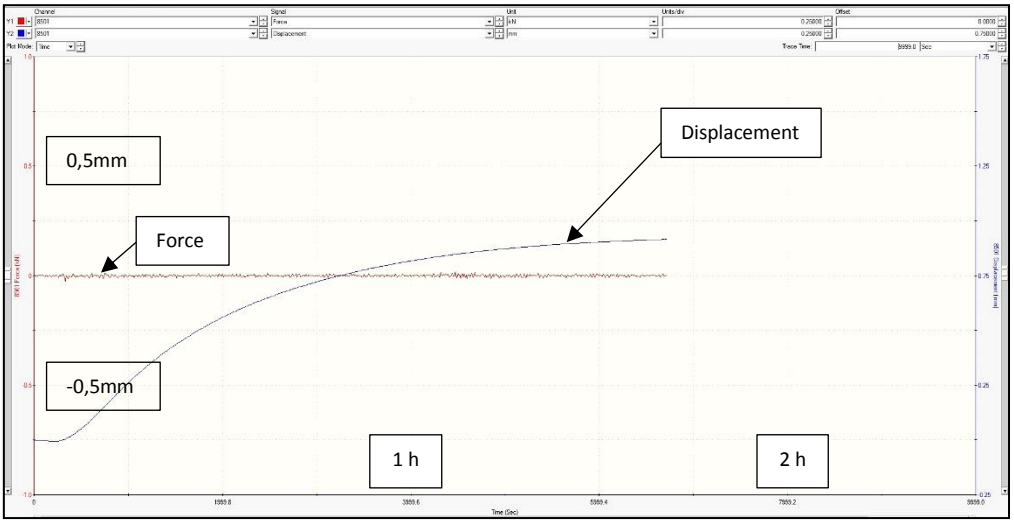

Figure 6: Temperature stabilization of the equipment

With equipment and sample expansion being significant, it is imperative that the heat up and stabilization procedures are followed rigorously to avoid interference from the equipment expansion on the measured sample deformation during the tests. The material ages when subjected to the elevated temperatures during the equipment stabilization before the high temperature tests commence. Internal studies [20] on the material ageing characteristics of the A356 + 0.5 % Cu - T7 heat treated material is summarized in Figure 7. The material exhibits decreasing strength with increasing heat treatment temperatures and times at temperatures above 150 °C.

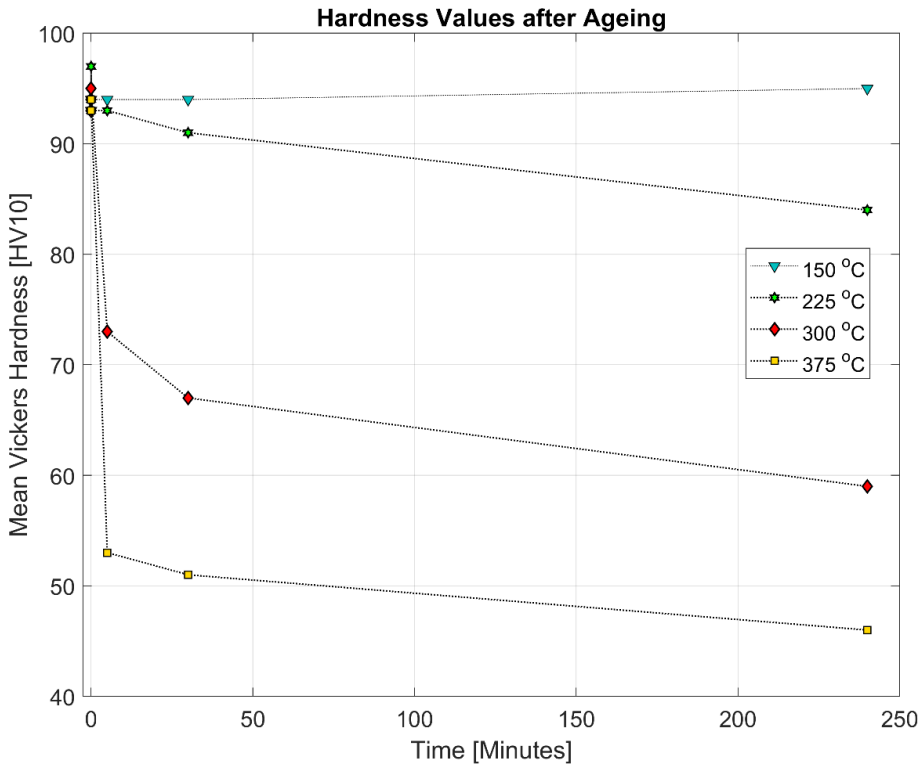

Figure 7: Ageing curves developed using Vickers hardness test (HV10)

The rate of material softening is higher for higher temperatures. With the above phenomenon in mind, the effect of the 3-hour hold time for the equipment temperature stabilization can be summarized as in Figure 8 and Figure 9. The samples subjected to the 3 hours hold time at temperatures above 150 °C are expected to develop a lower stress response for the applied loads as against the ideal test condition in which the samples are loaded without the need for a high temperature hold for equipment stabilization. Higher the test (and consequently, the stabilization) temperature, greater is the expected material softening. All the test results (deformation and lives) presented in subsequent sections are of specimens that have been aged for 3 hours at the stated isothermal temperatures prior to testing.

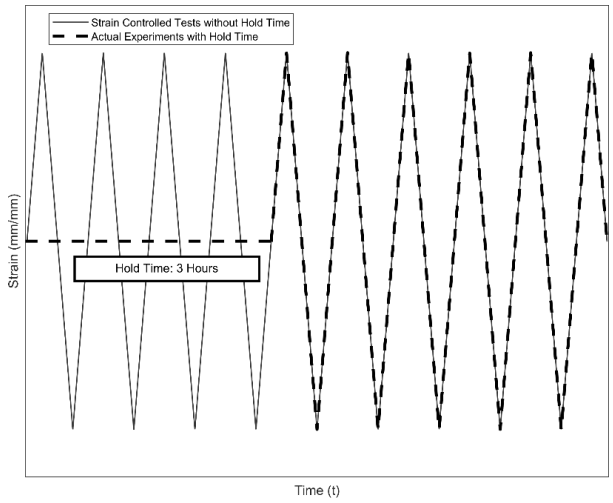

Figure 8: Load application in strain controlled LCF tests with and without hold time

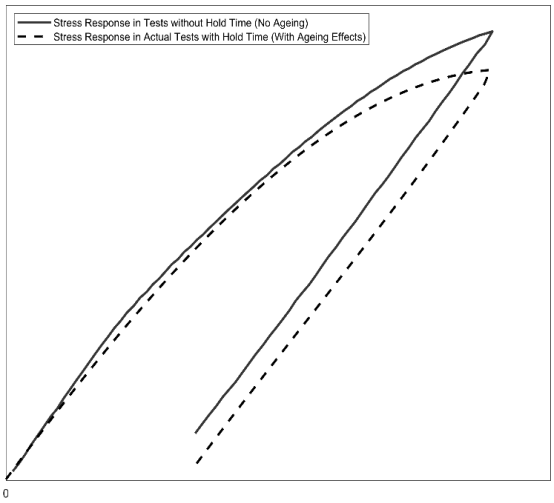

Figure 9: Stress response in strain controlled LCF tests with and without hold time

4. Results and Summary of Appended Papers

A summary of the results and analysis contained in the appended papers is briefly presented in this section.

4.1 General Observations

A scatter in the mechanical deformation and fatigue properties is expected because of the specimens being extracted from different locations on the cylinder heads with differing cooling rates and consequently, with varying microstructure. In addition, there exists a possibility of variations arising on account of the source of the samples being multiple batches of castings with several moulds used in the production process at the source foundry [15]. These variations are primarily observed in the dendritic arm spacing (both primary and secondary) of the specimen microstructure [63] resulting in non-uniform mechanical properties as evidenced in the following sections.

It is also important to register that all high temperature tests were carried out after a 3 hour isothermal dwell at the test temperatures for equipment stabilization before the tests commenced. Internal studies [20] and those presented in literature [64] of temperature effects in A356 + 0.5 % Cu - T7 alloys have shown material over-ageing at temperatures above 150 °C. As such, all the presented results at temperatures above 150 °C are expected to be influenced by the pre-ageing equivalent to over-ageing of 3 hours at the tested temperatures.

4.2 Monotonic Deformation

Figure 10 shows the stress development for strain controlled monotonic deformations of multiple replicas at isothermal temperatures while strained at a strain rate of 0.01 % sec^{-1}. All samples exhibit a gradual change from elastic deformation to plastic deformation without a distinct yield point. Since the deformation values are large, the true stresses and strains are preferred for the evaluation of the tensile curves. The observation of the test results at various temperature indicate a reduction of the tensile (and yield) strength of the material with increasing temperatures. With the softening of the material, the ductility correspondingly increases with increasing temperatures and goes over 17 % at 300 °C without tensile fracture.

Cast structures often have an inhomogeneous variation of the cooling rate through the structure because of which the microstructure, the secondary dendritic arm spacing in particular, varies across the cast structure. Numerous studies have shown the effect of the variation of the dendritic arm spacing on the resulting deformation properties [37], [44], [51], [63], [65]. Studies on the extracted material before the mechanical tests showed a maximum variation in the dendritic arm spacing of about 5 % across the valve bridge area. The scatter in the deformation behaviour between replicas can possibly be attributed to this microstructural variation between the samples. It is also of interest to note that the scatter is much less pronounced at temperatures at and above 250 °C. The results of the tensile tests are summarized in

Table 2. The stiffness, yield strength and the tensile strength all decrease with increasing temperatures with a rather sharp fall in properties at the highest tested temperature of 300 °C. Also, of interest is the increasing strain reached before fracture at higher temperatures with the ductility at 300 °C being almost 4 times than at room temperature.

Monotonic tests of A356-T6 at room temperature documented in [66], [67], show a higher yield and tensile strength in the range of 270 MPa and 330 MPa respectively on account of the material being peak aged. Studies have shown that over-ageing leads to coarsening of the precipitates and consequently provide less resistance for dislocation motion and hence, a reduction in strength is often observed in over-aged A356 alloys [21]. Deformation studies by Zhu et al. [37] on A356-T6 alloys without copper show a tensile strength in the range of 150-179 MPa and UTS in the range of 250-285 MPa with higher ductility (5-10 %) exhibiting a lower yield strength, but higher tensile strength and elongation in relation to the A356 + 0.5 % Cu - T7 that was tested in this study.

While A356 could indicate a wide latitude of chemical compositions, a rule of thumb to translate the tensile test results could be as summarized by Caceres et al. [33]: Increasing magnesium or copper tends to increase the flow stress while reducing the ductility of the material. Increased iron tends to reduce both the strength and ductility of the material. A decrease of the SDAS (areas with lower solidification rate) typically leads to a reduction of ductility and ultimate tensile strength while the yield strength and the strain hardening rate tend to be weakly affected [33].

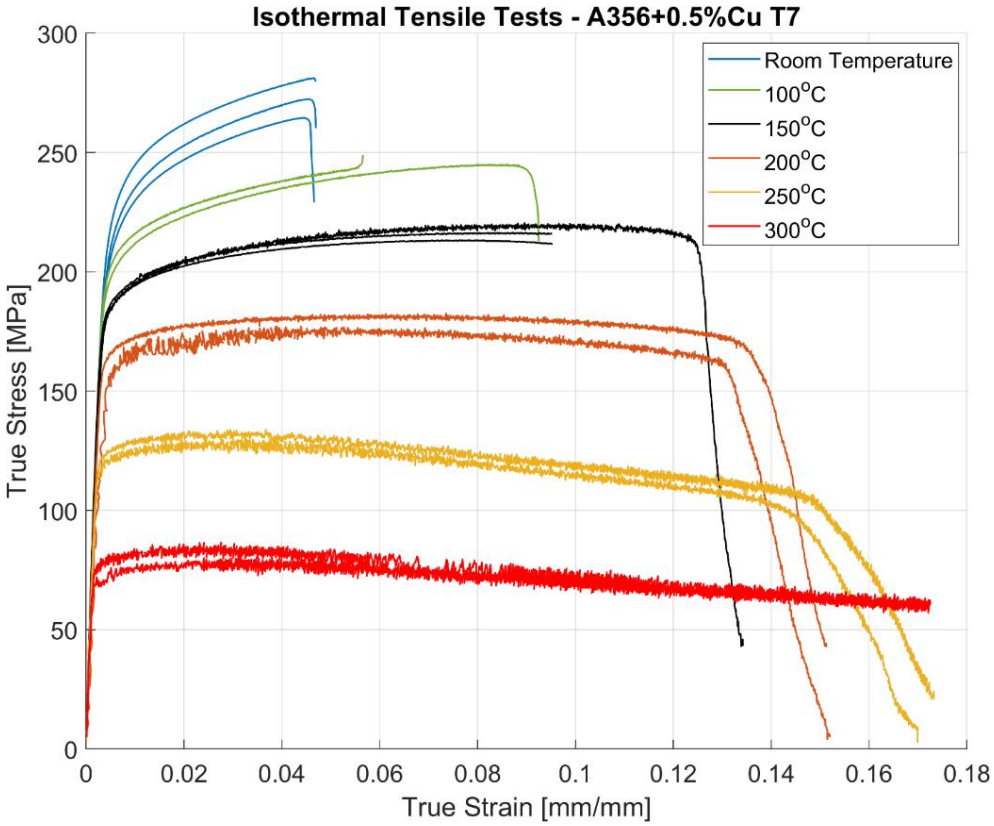

Figure 10: Isothermal Tensile Monotonic Test Results

Table 2: Summary of tensile test properties

Temperature °C	Young's Modulus E [GPa]	Offset Yield Strength R_p 0.2 % [MPa]	Ultimate Tensile Strength R_m [MPa]	Maximum Strain Before Fracture ε_f [%]
RT	71.94	210.68	272.76	4.682
100	70.64	198.54	246,97	7.453
150	70.22	183.61	216.73	13.420
200	64.13	157.90	179.88	15.165
250	60.82	122	132.52	17.16
300	56.06	73.37	83.87	>17.2 %

The deformation behaviour in Al-Si cast alloys is often rationalized by considering them akin to metal matrix composites [68] with α-Al acting analogous to the matrix and the eutectic Si, Mg, Cu, Mn, Fe intermetallics acting like the reinforcing phase [33]. During the deformation, as the particulate intermetallics remain elastic, a stress incompatibility is generated between the intermetallics and the soft matrix. A plastic relaxation occurs near the tip of the intermetallics with further deformation. At lower temperatures, it is reasonable to assume that the load shedding to the precipitates is higher and the intermetallics crack earlier before the commencement of plastic relaxation compared to corresponding strains at elevated temperatures thus reducing the ductility of the material with decreasing temperatures.

4.3 Cyclic Deformation

4.3.1 True Stress Peaks Evolution

Figure 11 shows the development of the peak tensile and compressive true stresses developed over each strain load cycle through the life for the three replicas tested at each of the three completely reversed strain loads with amplitudes of 0.2, 0.3 and 0.4 % at different temperatures. The stress range increases with successive cycling of the prescribed strains indicating a cyclic hardening behaviour of the material at room temperature and softening at higher temperatures with the material softening rate increasing with increasing temperatures. While the material hardens or softens cyclically, it does so with some asymmetry between the peak tensile and compressive stresses as shown in Figure 11. The material seems to exhibit a Bauschinger like effect [69] with higher peak compressive stress recorded for all the cases and with all the tests started with loading in tension from the no-load condition.

The peak stress values towards the end of the life of a component is often times influenced by the position of the crack relative to the extensometer blades [70]. A major crack within the two extensometer blades often results in the peak tensile stress decreasing near failure while on the other hand, it increases if the crack is positioned outside the blades in a strain controlled test. For the latter case with the crack outside the gauge length of the extensometer, the machine applies excess load near the end of its life to enforce the prescribed strain cycles in the volume between the extensometer blades resulting in a faster fracture. This could potentially explain the increase or fall in the peak stresses developed closer to the final fracture of the specimens. The scatter in the stress response between identical replicas decreases with increasing temperatures just as with the monotonic deformation response presented above indicating the decrease in influence of the microstructure on the deformation properties with increasing temperature. As can be expected, the flow stresses are reduced at higher temperatures than at lower temperatures for corresponding loads. As with most metals [12], the softening is more prominent in the initial stages of the cyclic loading especially at higher strain loads.

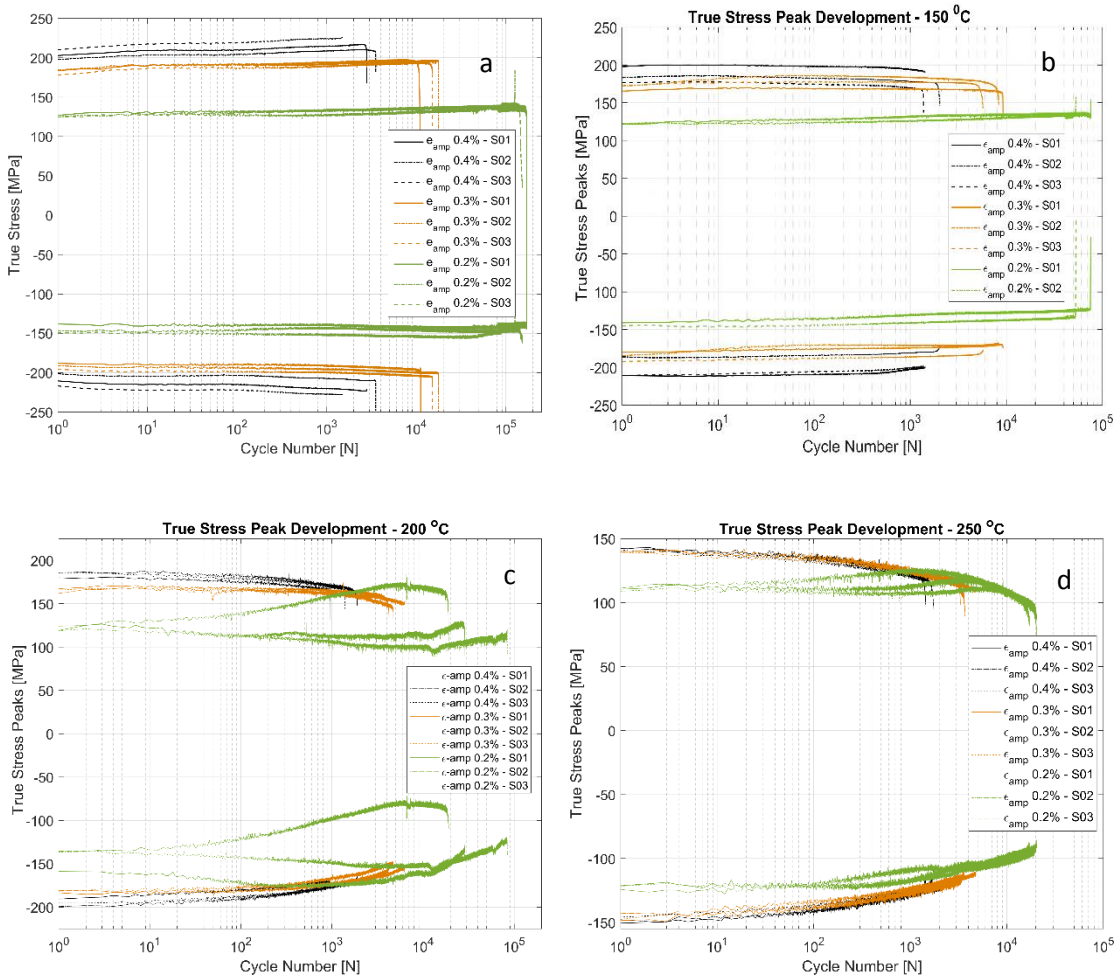

Figure 11: True tensile and compressive peak stress evolution through the life of strain controlled LCF tests at different temperatures a) Room temperature tests, b) Tests at 150 °C, c) Tests at 200 °C and d) Tests at 250 °C

4.3.2 Mean Stress Relaxation

Assembly loads and operational loads can often lead to initial strains in the cylinder head [66] and hence, it becomes imperative to explore the effect of biased cyclic loads ($R_\varepsilon \neq -1$) on the cyclic deformation behaviour. To study the effect of biased strain peaks in strain controlled cyclic loading, two strain cycles with one between $\varepsilon_{max} = 0.6$ % and $\varepsilon_{min} = -0.2$ % and the other within the strain limits between $\varepsilon_{max} = 0.2$ % and $\varepsilon_{min} = -0.6$ % was applied and the resulting mean stress development is presented in Figure 11. The material exhibits the so-called cycle-dependent relaxation or otherwise known as mean-stress relaxation. A stable mean stress is not achieved during the life of the specimen and the material continues to relax with a strong initial relaxation that reduces gradually as the cyclic loading progresses. Figure 11 and Figure 12 show the interplay between cyclic hardening and the mean stress relaxation. While the material does harden, the cycle dependent relaxation plays a more dominant role resulting in the stress peaks dropping over time as can be seen in Figure 12.

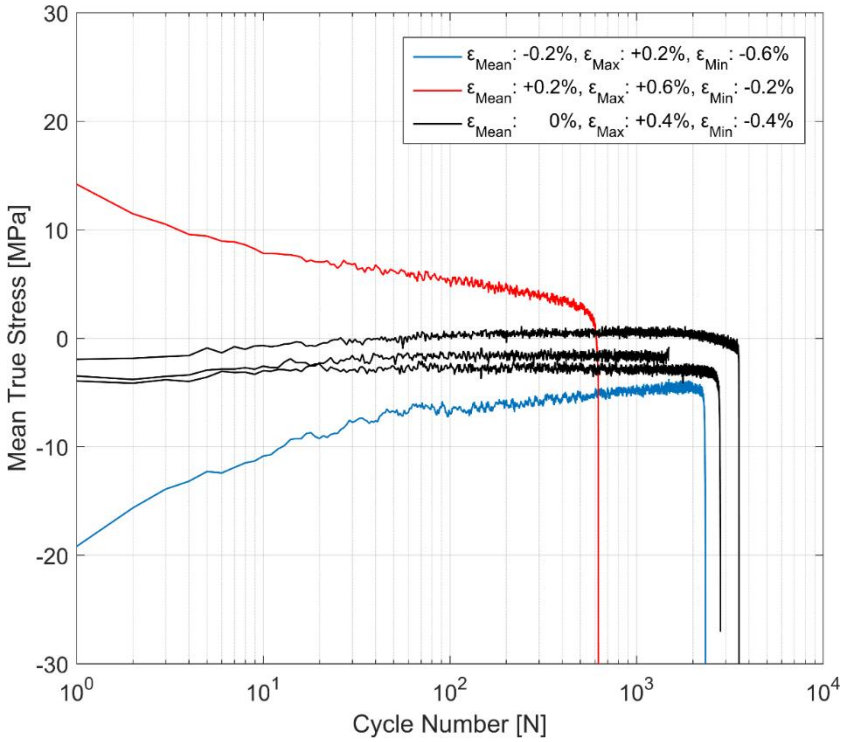

Figure 12: Effect of mean strain on the mean stress development in strain controlled LCF

4.3.3 Plastic Strain Amplitude Evolution

An alternative way to look at the material cyclic hardening or softening behaviour is to observe the evolution of the plastic deformation with cyclic loading. As can be seen in Figure 13 (a), the plastic strain range at room temperature keeps decreasing with successive strain load cycling for all strain levels and specimens. While the cyclic softening indicated by the increase in the developed plastic strain amplitude is almost negligible at 150 °C, the notion that softening increases with increase in temperatures is further evidenced by the evolution of the plastic strain amplitude at 200 and 250 °C. The material demonstrates an initial steeper hardening or softening behaviour followed by decreasing hardening or softening rate with subsequent load cycles especially for the low temperatures and with the softening response appearing fairly linear at elevated temperatures.

Just like the stress response in monotonic and cyclic loading, the plastic strain amplitude evolution exhibits a lower level of scatter between identical replicas at temperatures above 200 °C. The applied load levels don't seem to have a significant effect on the rate of hardening or softening with all three load levels indicating similar trends in hardening and softening through the life of the component. The material exhibits insignificant plasticity at the lowest strain load level of 0.2 % and increases significantly to contributing to more than half the applied strain at 250 °C.

Takahashi et al. [21] observed an increasing plastic strain amplitude when testing under thermo-mechanical fatigue conditions on account of the over-ageing of A356 - T6 samples. In line with the argument, one can expect the over-ageing of the tested material during the isothermal high temperature hold times associated with the equipment stabilization and a corresponding time dependent softening response before the high temperature strain load cycles are started.

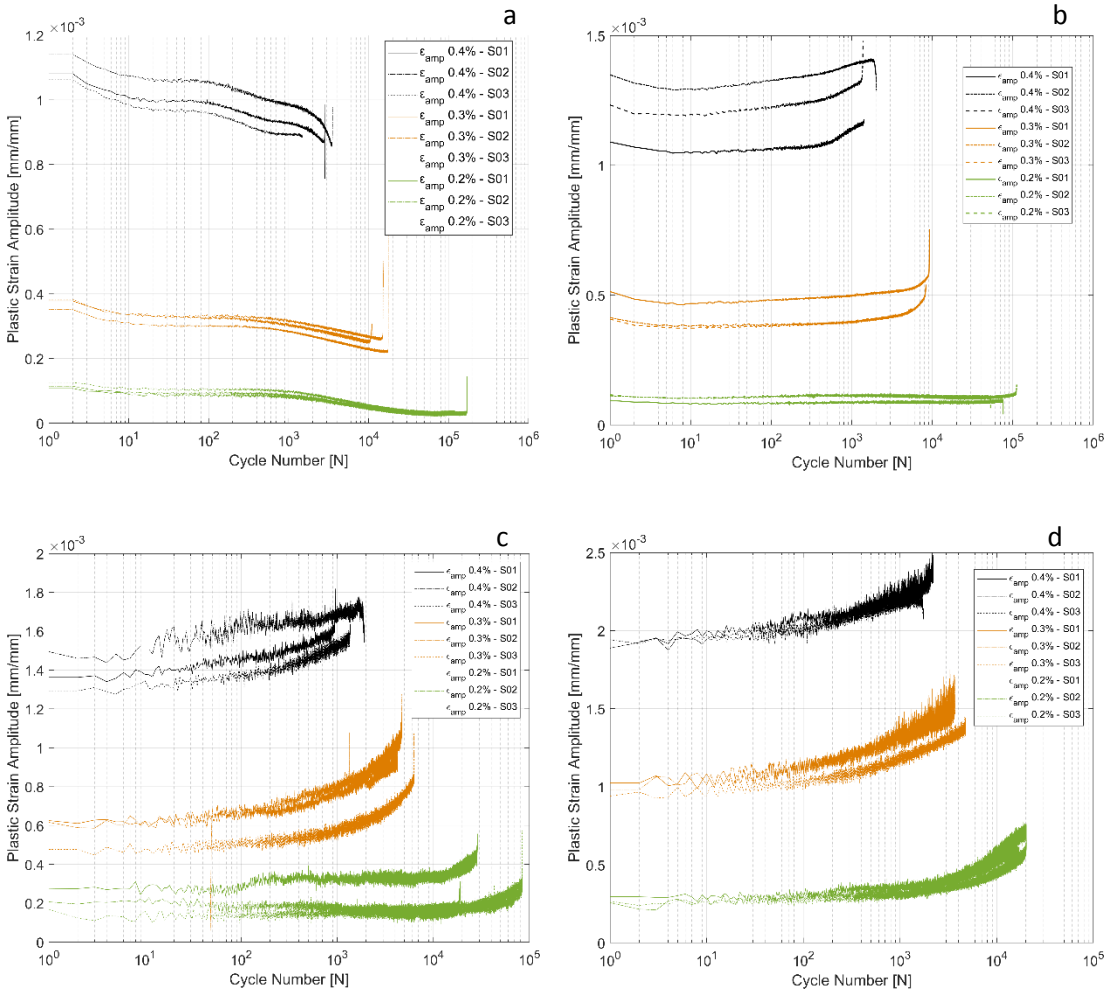

Figure 13: Evolution of plastic strain amplitude with cyclic strain controlled loading at different temperatures a) Room temperature tests, b) Tests at 150 °C, c) Tests at 200 °C and d) Tests at 250 °C

4.3.4 Hysteresis Loops

4.3.4.1 First Cycle Hysteresis Loops

The first cycle hysteresis loops presented in Figure 14 shows the cyclic deformation for the various strain-controlled tests at different loads and temperatures. The slopes of the hysteresis loops at isothermal temperatures show slight variation at lower temperatures between different load levels and between replicas at identical loads. Like with most of the deformation properties presented before, the difference in the deformation behaviour between the replicas at different load levels decreases with increasing temperatures indicating the waning influence of the microstructure on the deformation properties with increasing temperatures. An increasingly softening response is exhibited by the material with increasing temperatures as indicated by the decreasing peak stresses and the widening of the plastic strain amplitude indicated by the width of the hysteresis loops.

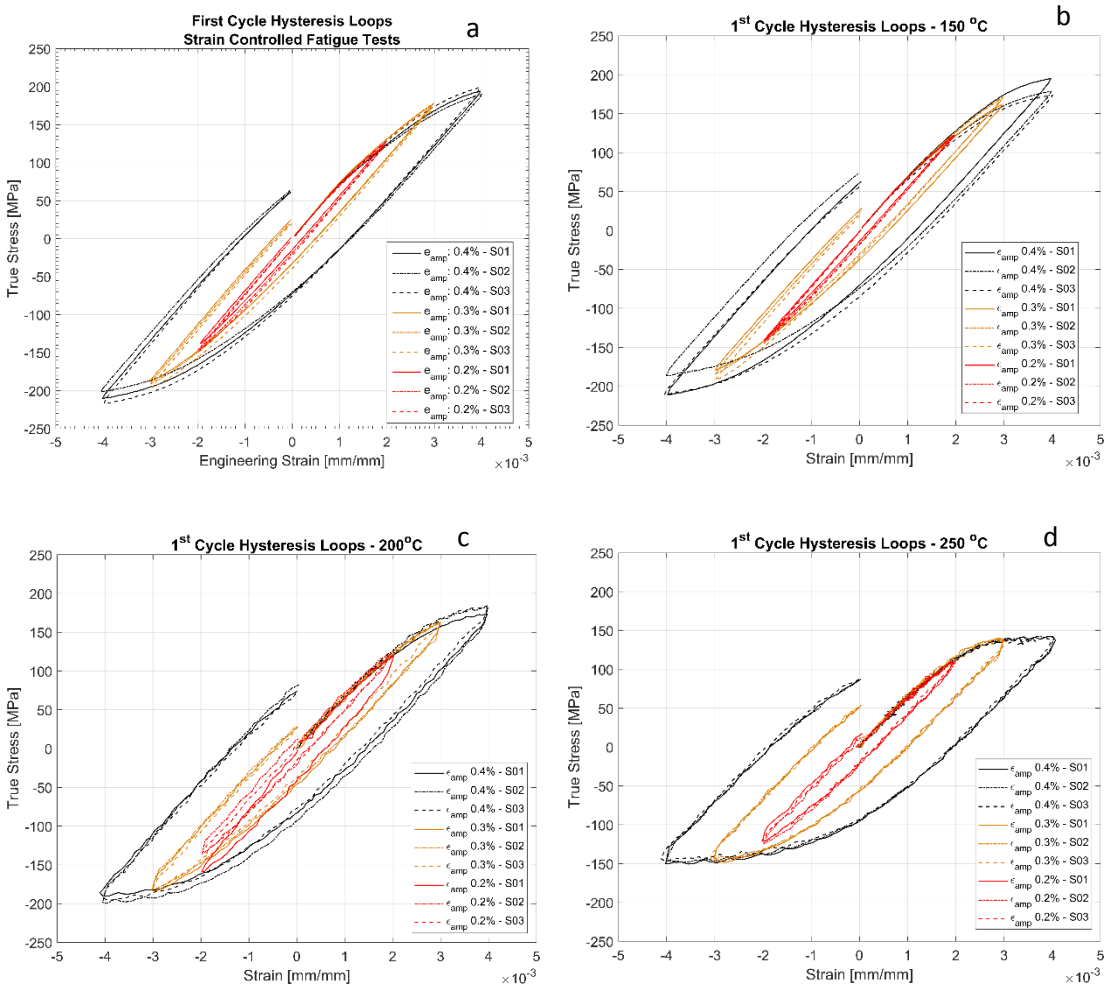

Figure 14: First cycle hysteresis loops of strain controlled LCF tests at a) Room temperature, b) 150 °C, C) 200 °C and d) 250 °C

4.3.4.2 Half Life Hysteresis Loops

A comparison of the first load cycle presented in Figure 14 and the hysteresis loops at half the life presented in Figure 15 show the hardening behaviour evolution of the A356-T7 + 0.5 % Cu alloys at different temperatures. The material exhibits significant hardening at room temperature as indicated by the hysteresis loops becoming almost fully elastic at the strain load cycles between ± 0.2 % at half the life. At 150 °C, the stress response and the plastic strain amplitudes exhibit a trivial difference indicating insignificant cyclic hardening or softening response. At further high temperatures of 200 °C and 250 °C, the material exhibits significant softening with the plastic strain range increasing in width with increasing temperatures also indicating a temperature dependent softening. However, the strain load level dependence of the hardening slopes and the deformation difference between replicas tend to decrease with increasing temperatures indicating the waning influence of the microstructure at higher temperatures.

Also, of interest is the differing hardening slopes between the strain levels at half-life compared to the first cycle hysteresis loops where the initial deformation slopes are similar. From Figure 14 and Figure 15, we can observe that a strain load level dependent hardening exists for temperatures up to 200 °C indicated by the differing deformation slopes of the half-life hysteresis loops compared to the corresponding first cycles. At the highest tested temperature of 250 °C, all the strain load levels exhibit similar hardening behaviour. This load dependent

hardening behaviour at temperatures below 250 °C shows similarities to studies by Snowden [71] and Grosskreutz [72]. Snowden [71] studied the dislocation arrangements in aluminium crystals during cyclic hardening and observed that the ratio of the Bauschinger strain to the total applied strain amplitude increased with decreasing strain amplitudes. This higher reversibility of dislocations (Bauschinger effect) at small strain amplitudes, he contends, is a probable explanation for the marked difference in the hardening behaviour at differing strain amplitudes. Grosskreutz [72] also observes a differing dislocation structure depending on the applied strain levels. At low strain levels, during the hardening stage, the density of the dislocation bundles was found to increase while the spacing between them decreased and with most of the dislocations belonging to the primary system. At higher applied strain amplitudes, the dislocations within these bundles were fragmented to shorter lengths with the density of dislocations in the secondary slip system being increased and a rough three-dimensional structure was built up. The non-linear nature of hardening is explained by the negligible concentration of the point defects and clusters in the initial cycles that become significant at later stages and influence the flow stress by exerting increased frictional drag on the dislocation motion.

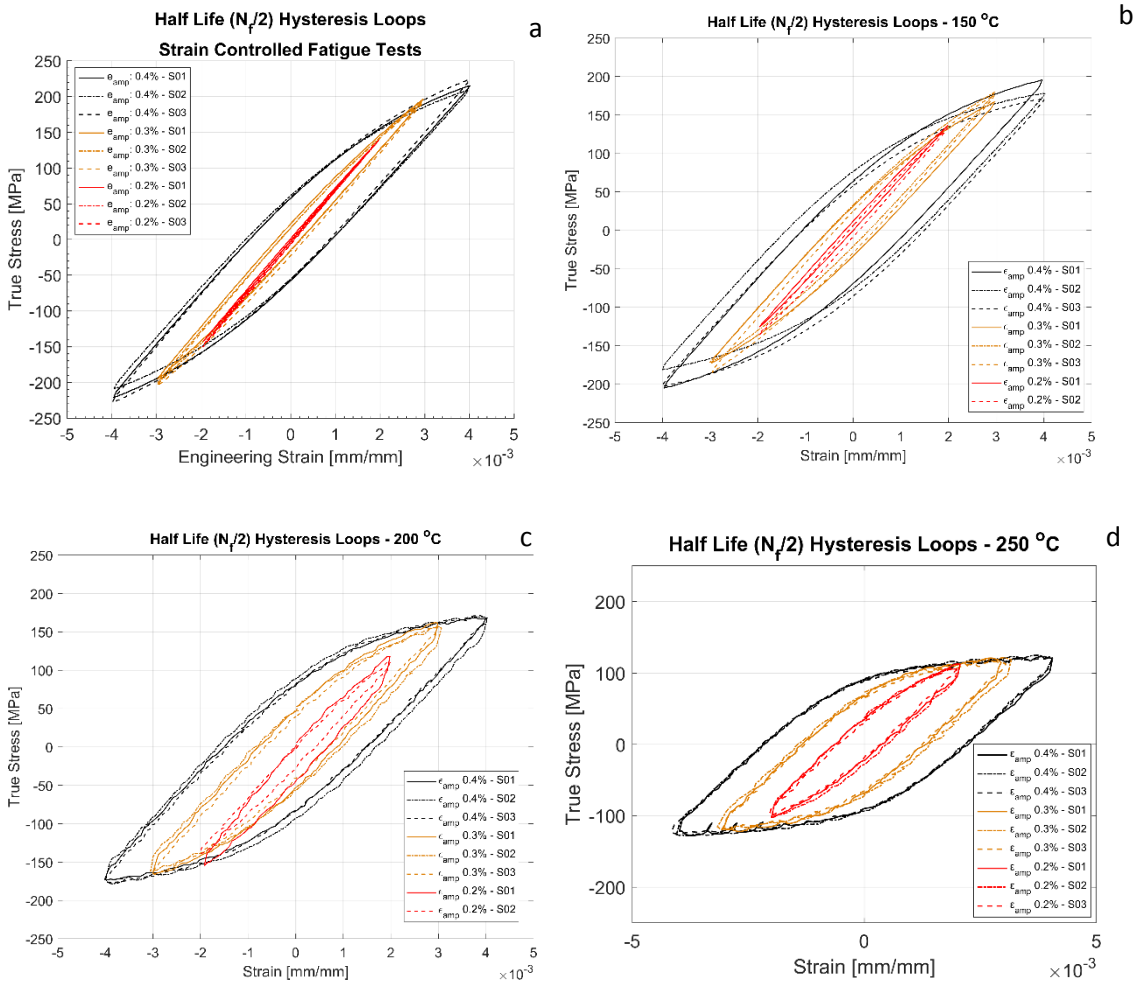

Figure 15: Hysteresis loops at half-life of strain controlled LCF tests at a) Room temperature, b) 150 °C, C) 200 °C and d) 250 °C

4.3.5 Numerical Models for Cyclic Deformation

4.3.5.1 Ramberg Osgood Model for Cyclic Hardening

The cyclic hardening curve is usually used to represent the stable stress response to cyclic strain loads and vice versa. Cyclic stress-strain curves are usually drawn through the stress-strain peaks obtained at the half-life of the strain or stress controlled fatigue tests [12]. Since the tensile and compressive load peaks are asymmetric as can be seen in Figure 15, their numerical mean is used for developing the cyclic hardening curves representing relationship between the stress and strain amplitudes for the cyclic loading of the tested A356-T7 alloy. As there is no distinct yield point of the cyclic stress strain curve, as is often the case with cyclic hardening curves [12], a Ramberg-Osgood type equation is used to model the cyclic stress-strain curve.

For the room temperature tests, as the plastic strain amplitudes obtained at 0.2 % strain amplitude tests and the equivalent stress-controlled tests are low, hence, only the plastic strain amplitudes obtained at the higher loading levels of 0.3 % and 0.4 % strain amplitudes and the corresponding stress-controlled test data were calibrated against the Ramberg-Osgood model. It can be seen from Figure 16 and Table 3 that the difference between the cyclic hardening curves obtained from the stress and strain controlled fatigue tests could be considered equivalent because of what could be considered an insignificant difference in the stress and strain amplitudes obtained from the two types of tests. Azadi et al. [66] studied the differences between the monotonic hardening behaviour of A356 - T6 alloys between stress and strain controlled loadings and observed no discernible differences. A similar indifference in the cyclic hardening behaviour is observed here for the over-aged A356 - T7 alloys.

The material exhibits a higher stress response for increasing train load levels for all the tested temperatures. Alloy processing has been shown to have a profound effect on the cyclic stress-strain behaviour. Metals that have been softened by heat treatment (like the over aged T7 temper in the present case) and precipitation hardened aluminium alloys in general often tend to harden with increasing strain amplitudes when cyclically loaded.

Ramberg-Osgood Cyclic Stress-Strain Model:

$$\varepsilon_{amp} = \frac{\sigma_{amp}}{E} + \left(\frac{\sigma_{amp}}{H'}\right)^{\frac{1}{n'}}$$

Here σ_{amp}, ε_{amp} being the stress and strain amplitudes respectively. H' and the cyclic strain hardening exponent n' are different from monotonic curves and are determined using the least squares fitting of the test data to expression as shown below:

$$\sigma_a = H' \varepsilon_{pa}^{n'}$$

The offset yield strength σ_0' for the cyclic stress-strain curve is obtained by substituting a plastic strain amplitude of 0.002 in the expression obtained above. The obtained values for the cyclic stress-strain curves are presented in Table 3.

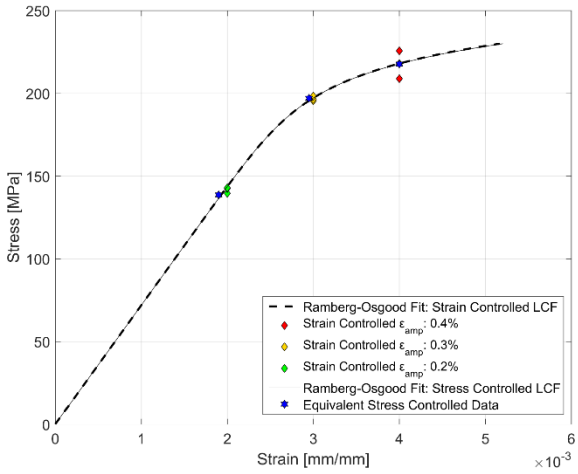

Figure 16: Ramberg-Osgood cyclic hardening model of stress & strain controlled LCF tests at room temperature

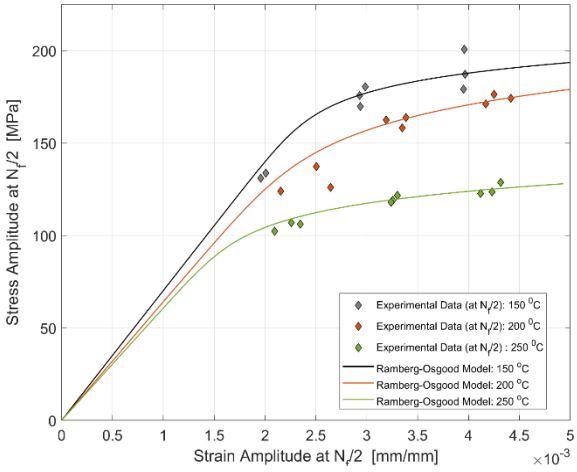

Figure 17: Ramberg-Osgood cyclic hardening model of strain controlled LCF tests at elevated temperatures

Table 3: Ramberg-Osgood cyclic hardening model parameters

Test Temperature	Young's Modulus [GPa]	Offset Yield Strength σ_0' [MPa]	H' [MPa]	Cyclic Strain Hardening Coefficient n'
RT	71.94	230.25	368.79	0.0758
150 °C	70.22	192.30	274.39	0.0572
200 °C	64.13	177.37	321.10	0.0955
250 °C	60.82	124.11	215.65	0.0889

4.3.5.2 Cyclic Plasticity Modelling

For the design and analysis of structures, one often needs a constitutive model of the material that the structure is made of. A constitutive model is a mathematical simplification that relates the state of stress and strain in the material. While a number of different physical behaviour could be modelled, one often chooses a degree of complexity that is adequately accurate for the phenomenon of interest without becoming inessentially complex and computationally expensive [73].

The tensile and compressive stresses in Figure 14 and Figure 15 indicate that the stresses are asymmetric about the no load axis with stresses in compression slightly higher than in tension at the corresponding peak strain loads. This indicates the need for a kinematic hardening model that takes in to account the translation of the yield surface when the load directions are changed. The plastic strain amplitude presented in Figure 13 also indicates a constant change in the yield surface with cyclic hardening exhibited at room temperature and significant softening observed at temperatures above 200 °C. This necessitates an isotropic hardening model to be combined with the kinematic hardening model. The hysteresis loops obtained also exhibit differing hardening rates with the hardening in the initial cycles eventually decreasing to a saturation value indicating that a non-linear combined isotropic and kinematic hardening is quite suitable to model the cyclic deformation behaviour of the tested A356 + 0.5 % Cu - T7 material.

Such a rate independent non-linear combined isotropic-kinematic hardening model as implemented in a commercial FE software like Abaqus [20] is used in this study to identify the model parameters. The model consists of a non-linear kinematic hardening term and an isotropic hardening component.

Non-Linear Kinematic Hardening Model

The kinematic component consists of a pure kinematic term based off of the linear Ziegler hardening law and a recall term that introduces the non-linearity. The model implemented has two kinematic backstresses that are superposed (one linear and one non-linear term) to get better predictions. The linear Ziegler hardening law with multiple backstresses is defined as below [74]:

Kinematic Hardening Law:

$$\dot{\alpha}_k = C_k \frac{1}{\sigma^0}(\sigma - \alpha)\dot{\bar{\varepsilon}}^{pl} - \gamma_k \alpha_k \dot{\bar{\varepsilon}}^{pl}$$

Overall backstress**:**

$$\alpha = \sum_{k=1}^{2} \alpha_k$$

Where, C - initial kinematic hardening moduli and γ determines the rate at which the kinematic hardening moduli decreases with increasing plastic deformation.

Non-Linear Isotropic Hardening Model

The change in the size of the yield surface is modelled using an exponential law [74] as below:

Exponential Law:

$$\sigma^0 = \sigma_{|0}^{|} + Q_\infty \left(1 - e^{-b\bar{\varepsilon}^{pl}}\right)$$

Where, $\sigma_{|0}^{|}$ - Yield at zero plastic strain
Q_∞ - Maximum change in the size of the yield surface
b - Rate at which the size of the yield surface changes as plastic straining develops.

$C_k, \gamma_k, \sigma_{|0}^{|}, Q_\infty,$ b are all the material parameters that are calibrated against cyclic test data. The temperature dependent model parameters are determined by minimizing the root mean square of the error between the experimental data and the simulated response using the Nedler-Mead optimization algorithm. The cost function for minimizations is as shown below:

$$F(\pi) = \frac{1}{2} \sum_{i=1}^{N} [\sigma_i(\pi, t_i) - \bar{\sigma}(t_i)]^2$$

With σ_i being the simulated value and $\bar{\sigma}$, the experimental response. The data is sampled at different time intervals t_i equating to identical strain load levels in the simulated and experimental response. The model parameters are calibrated against test data of the first 20 cycles of strain controlled LCF tests with ε_{amp} = 0.4 % and a strain ratio of R_ε=-1 at all the different tested temperatures. The model is calibrated against one set of experimental data at each temperature and the summary of the obtained model parameters is presented in Table 4. The results of the inverse parameter identification showing the 20th cycle of the experimental data against the simulation results obtained from commercial FE software Abaqus are presented in Figure 18 (a), (b), (c), and (d) for the strain controlled tests at room temperature, 150, 200, and 250 °C respectively.

The temperature dependent model parameters are obtained by calibrating the model against the test data from room temperature and using the obtained values as the starting values in the optimization procedure for 150 °C and so on. The optimization routine is constrained to obtain sequentially varying values to get predictable interpolation at temperatures in between the tested and modelled values. Such constraining is often necessary to avoid obtaining local minima that would otherwise lead to unpredictable interpolations.

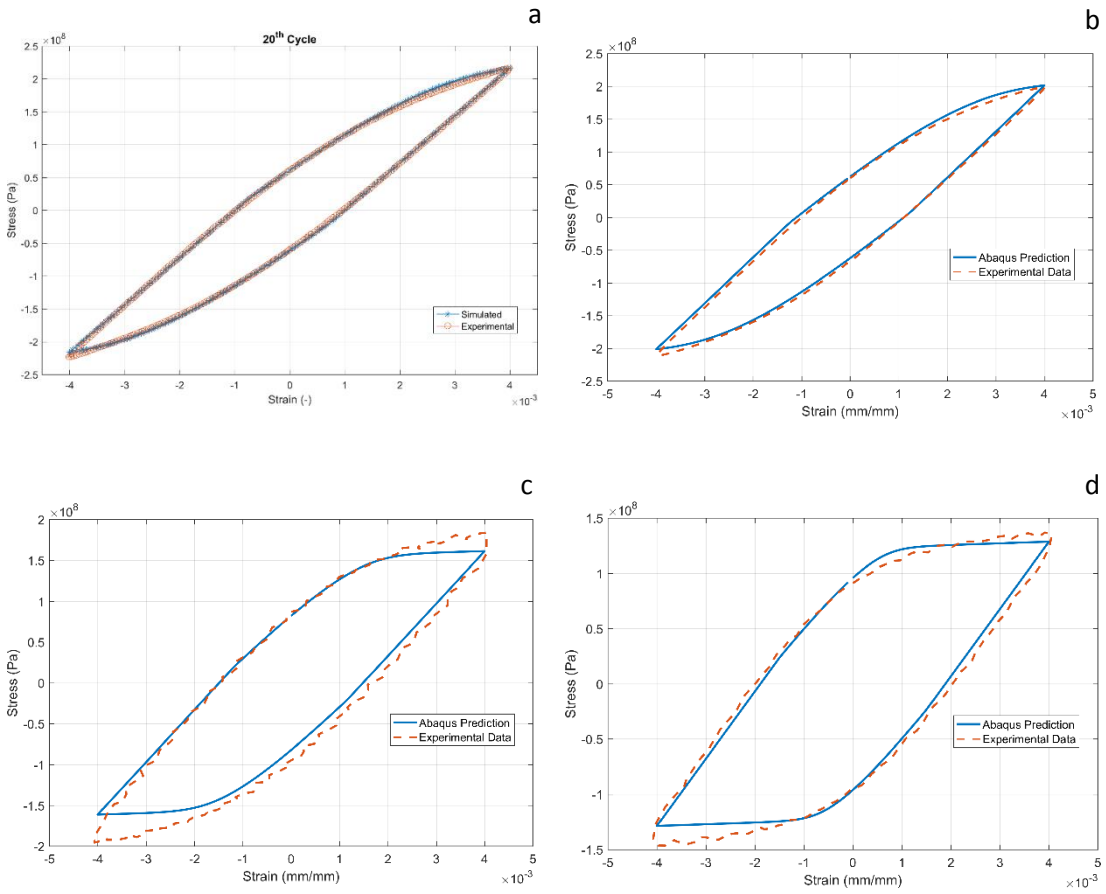

Figure 18: Model Prediction vs Experimental Data of the 20th Strain Cycle from the LCF Tests at a) Room Temperature, b) 150 °C, c) 200 °C and d) 250 °C

Table 4: Model parameters of the non-linear combined isotropic-kinematic hardening model

Temperature °C	Young's Modulus [Pa]	Yield stress at zero plastic strain & equivalent stress (for isotropic hardening model) [Pa]	Kinematic hardening parameter C1 [Pa]	Gamma 1 [-]	Kinematic hardening parameter C2 [Pa]	Gamma 2 [-]	Q-infinity [Pa]	Hardening parameter b [-]
RT	71.94e+9	1.108e+08	1.708e+11	1616	1.518e+09	0	55e+06	1.5
150	70.22e+9	9.967e+07	1.786e+11	1651	1.551e+09	0	-20e+06	2.0
200	64.13e+9	9.5e+07	1.997e+11	2933	1.569e+09	0	-20e+06	2.2
250	60.82e+9	8.2e+07	2.034e+11	4155	1.581e+09	0	-20e+06	2.3

4.3.5.3 Low Cycle Fatigue Life Models

On account of the local yielding and plasticity often involved in TMF, a strain-based approach to fatigue life prediction is frequently adopted in the automotive industry considering the cyclical nature of the thermal stresses associated with the engine start-stop cycle and the ductile nature of the aluminium alloys used in the IC engine. A temperature dependent strain life model is developed and can be employed to predict the TMF life of components. Most frequently, the parametric approach pioneered by Coffin [75] and Manson [76] is used to model the life of the

material as a function of the strain amplitude. While a continuum coupled damage approach as proposed by Chaboche [69] could also be used, the models often get complex while providing no improved life predictions [19], [25], [26]. The parametric models like the Coffin-Manson law are often adopted in the automotive industry because of its practicality while providing good life predictions [17].

The Coffin-Manson model parameters are determined from completely reversed strain-controlled fatigue tests (R_ε=-1) at different temperature. A strain life diagram with the Coffin-Manson modelling of the fatigue life for the room temperature tests is demonstrated in Figure 19 with the strain life model being an additive partition of the elastic and plastic strain components (i.e., $\varepsilon_a = \varepsilon_{ea} + \varepsilon_{pa}$). The elastic component (ε_{ea}) is determined from the stress amplitude and by using the Hooke's law while the plastic strain amplitude (ε_{pa}) is taken to be half the width of the half-life hysteresis loop.

The elastic relation is given by:

$$\varepsilon_{ea} = \frac{\sigma_a}{E} = \frac{\sigma_f'}{E}\left(2N_f\right)^b$$

The plastic relation is expressed as:

$$\varepsilon_{pa} = \varepsilon'_f (2N_f)^c$$

Coffin-Manson Relation:

$$\varepsilon_a = \varepsilon_{ea} + \varepsilon_{pa} = \frac{\sigma_f'}{E}\left(2N_f\right)^b + \varepsilon'_f (2N_f)^c$$

The obtained test data is modelled against the above relation and the model parameters as determined from the hysteresis loops at half the life [$N_f/2$] of the tested samples are presented in Table 5. Since the tests have been carried with low loads to obtain long lives, the obtained data can be used to predict lives where little plasticity is involved and long lives are expected to form a wide-ranging approach to fatigue life prediction. The two different life curves often dominate depending on the loading situation with the life curve aligning along the elastic strain-life line at long lives with a shallower slope and along the plastic strain-life line at short lives with steeper slopes as with most metals [12]. On observation, with increase in temperature, the ε_f' increases and the σ_f' decreases indicating an increasingly ductile behaviour with increasing temperatures.

Azadi et al. [66] studied the low cycle fatigue properties of the peak aged A356-T6 alloy with significantly lower copper addition (0.01 %) and on comparison, the fatigue lives reported at 250 °C are significantly lower at comparable strain levels in relation to the overaged A356 + 0.5 % Cu - T7 alloy studied here. The fatigue lives at lower temperature of 200 °C are comparable however indicating the potentially improved fatigue lives of the A356 alloy with higher copper content at elevated temperatures similar to improved monotonic deformation properties at temperatures above 250 °C as reported in various other studies [14], [77].

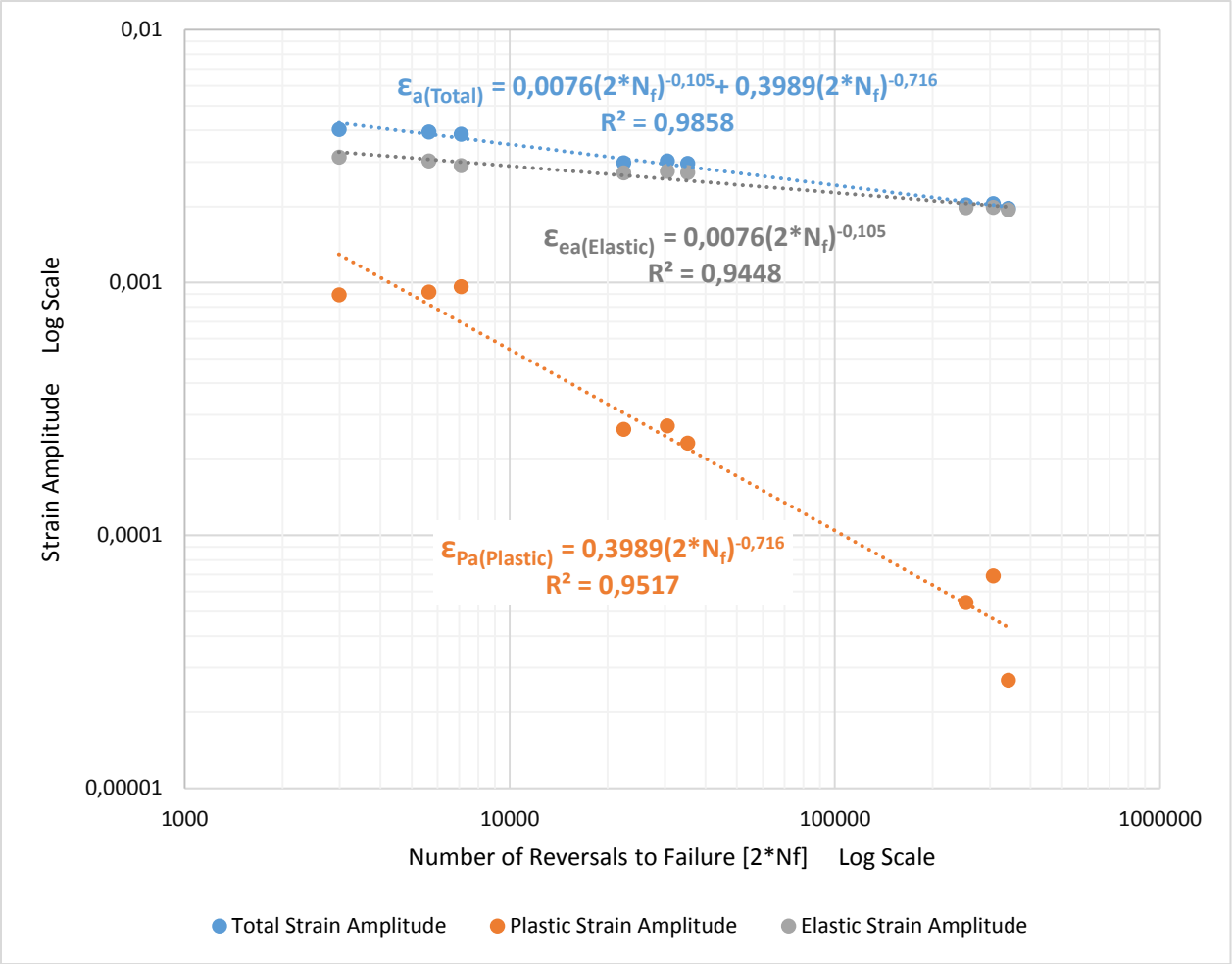

Figure 19: Strain life curves of A356-T7 at room temperature - Coffin & Mason relation

Table 5: Coffin-Manson model parameters for the strain-life curves

Parameter	E [GPa]	σ_f' [MPa]	b	ε_f'	c
RT	71.94	546.744	-0.105	0.3989	-0.716
150	70.22	421.32	-0.096	0.3069	-0.681
200	64.13	346.30	-0.087	0.0497	-0.441
250	60.82	231.12	-0.073	0.2774	-0.595

4.4 Dilatometry

The results of the dilatometry test to study the variation of the coefficient of thermal expansion with temperature is presented in Figure 20. The thermal expansion remains fairly stable through the temperature range with the coefficient of thermal expansion varying in between 25-26*10^{-6} °C^{-1} in the temperature range between 25 °C and 250 °C. The linear thermal expansion coefficient increases rapidly up to 31*10^{-6} °C^{-1} as the temperature increases further from 250 °C to 300 °C before receding with further increase in temperature. The measured thermal expansion values for the A356 + 0.5 % Cu - T7 alloy seems marginally higher than those reported by Grieb et al. [78] for similar group of alloys.

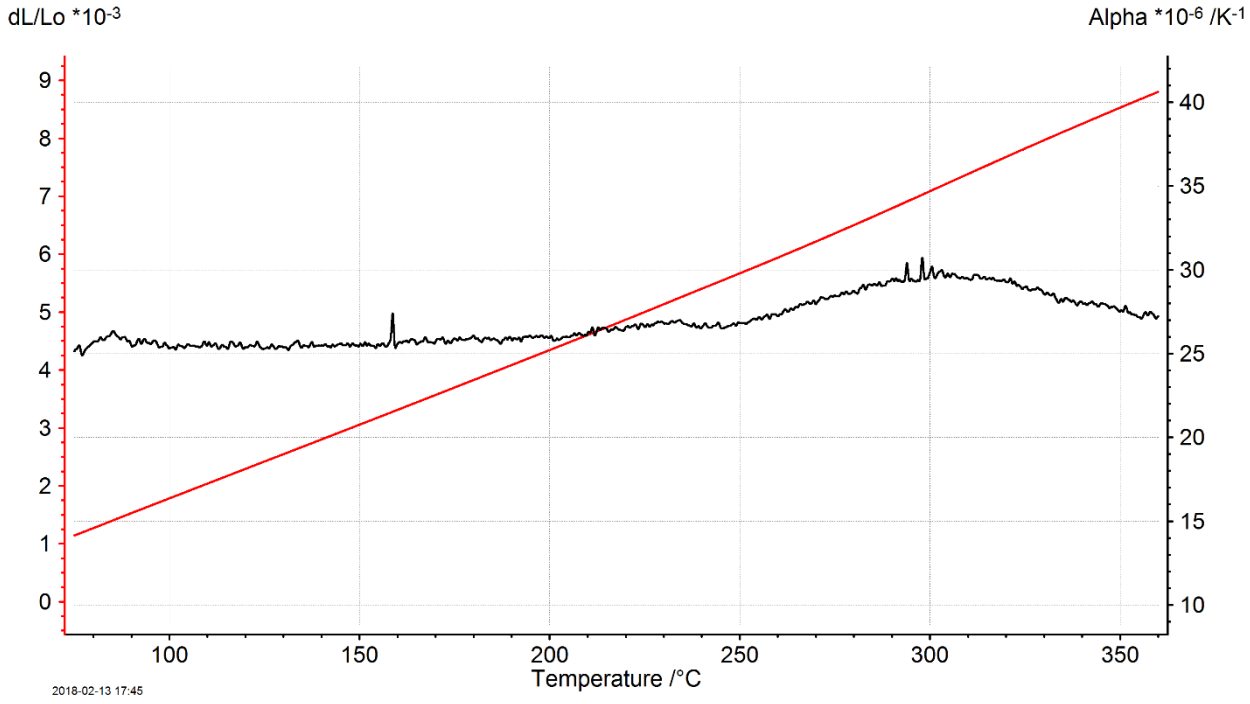

Figure 20: Variation of the coefficient of thermal expansion with temperature

5. Conclusions

The aim of the of the project is to study the deformation behaviour of the A356 - T7 + 0.5 % Cu alloys used in cylinder heads of the internal combustion engines that are part of the new hybrid powertrains at Volvo Cars. The project aims to develop constitutive and facture models that help predict the thermo-mechanical fatigue life of the highly loaded cylinder heads during the engine start-stop cycle.

This licentiate thesis work deals with testing and modelling the time independent plasticity in the temperature ranges of interest. Monotonic tensile tests are performed at various temperatures between the ambient room temperature and 300 °C. Strain controlled fatigue tests are carried out between ambient room temperature and the maximum expected material service temperatures of 250 °C in the internal combustion engine cylinder heads.

Under monotonic loading, the material exhibits decreasing strength and increasing ductility with increase in temperatures. Since the material doesn't exhibit a defined yield point, a Ramberg-Osgood type equation is used to model the tensile deformation behaviour.

Under cyclic loading, the material exhibits cyclic hardening at room temperature and cyclic softening at elevated temperatures. The continuum cyclic deformation behaviour of the material is modelled using a rate independent nonlinear kinematic-isotropic combined hardening model with one linear and one non-linear backstress. An initial survey of different fatigue criteria is also explored with particular emphasis on parametric and energy criterions often used with thermo-mechanical fatigue failures.

A dilatometric study is also carried out to capture the thermal deformation characteristics of the material subjected to varying temperatures often experienced in cylinder heads of internal combustion engines.

6. Future Work

1. Advance the material model developed by incorporating the time dependent visco-plastic deformation behaviour.
2. Conduct experiments to differentiate between cycle dependent and time dependent hardening and softening.
3. Explore and formulate efficient fracture models to predict the isothermal and thermo-mechanical fatigue life.
4. Explore the effect of ageing on the thermo-mechanical fatigue behaviour of the alloy and incorporate the ageing model with the constitutive model if necessary to improve fatigue life predictions.
5. Conduct various thermo-mechanical fatigue tests to verify the constitutive and fatigue life model predictions.
6. Gather and advance the knowledge of the A356 - T7 alloy microstructure and the temperature and deformation induced changes in the material.

7. Acknowledgements

I would like to express my sincere gratitude to my supervisors Prof. Christer Persson and Prof. Johan Ahlström for providing me with the opportunity to work on the project and for your endless patience, guidance, wisdom and support. I realise it's still a long road ahead, but I do hope to make you proud when the work eventually concludes!

The project is financially supported by FFI and the cylinder heads for testing were supplied by Volvo Cars whose contribution is gratefully acknowledged. I would also like to thank Stefan A Eriksson, Anders Thorell and Magnus Levinsson from Volvo Cars for their valuable feedback, guidance and time offered during the course of the project.

I would also like to express my appreciation for the interest Monika Vogler took in the project and the immense work that she has performed as part of her master thesis studying the ageing behaviour of the alloy. It has helped us better understand our material and will greatly influence most of our future work. Thanks for being such a great friend and the inspiring quality of work, it has definitely set the bar high for all our future work.

Sincere thanks also go to the research engineers in the department, in particular, Dr. Yiming Yao, Håkan Millqvist, Roger Sagdahl and Dr. Eric Tam for helping us to get the project up and running and for the experimental and technical assistance you so patiently provide to help us keep it that way.

Thanks to all the colleagues in the department I have had the privilege of sharing the workspace with, both past and present, for such a warm and inspiring work environment. And I would be remiss in my responsibilities if I fail to acknowledge all the little help that you so kindly provide with teaching, lab work and the experiments at every asking. There's so much more to be thankful for, but for the sake of brevity I will refrain from listing them all.

I would also like to gratefully acknowledge Knut Andreas Meyer for teaching me to work with the CNC lathe. I can't overstate how useful it has been to us so far. Your enthusiasm for all things engineering has definitely inspired me with my work since the formula student days. I would also like to thank Ali Esmaeli for his help and insight with the modelling work and his friendship.

And to wrap it off, great thanks to my girlfriend Pavi for her unconditional love and endless patience, I can't wait to start our life together. Thanks to all my friends and family for the support, love and encouragement all along.

8. References

[1] A. Raskin and S. Shah, “The Emergence of Hybrid Vehicles,” 2006.

[2] J. Gary Hawley, C. J. Brace, F. J. Wallace, and R. W. Horrocks, *Handbook of Air Pollution From Internal Combustion Engines*. 1998.

[3] Volvo Car Corporation, “TAKING THE LEAD: EMBRACING A CLEANER MOBILITY The Future is Electric.” [Online]. Available: https://group.volvocars.com/company/innovation/electrification.

[4] “PSA Peugeot Citroën’s DS Brand Will Sell Only Hybrids And Electric Cars Beginning in 2025 - The Drive.” [Online]. Available: http://www.thedrive.com/tech/20577/psa-peugeot-citrons-ds-brand-to-sell-only-electrified-vehicles-starting-in-2025?iid=sr-link10.

[5] “PSA Will Be ‘100 Percent Electrified’ by 2025 - The Drive.” [Online]. Available: http://www.thedrive.com/tech/17802/psa-will-be-100-percent-electrified-by-2025-ceo-says?iid=sr-link1.

[6] “Porsche’s first car, in 1898, was electric.” [Online]. Available: https://eu.usatoday.com/story/money/cars/2014/01/27/first-porsche-1889/4941635/.

[7] “The History of the Electric Car | Department of Energy.” [Online]. Available: https://www.energy.gov/articles/history-electric-car.

[8] “History of Hybrid Vehicles.” [Online]. Available: https://www.hybridcars.com/history-of-hybrid-vehicles/.

[9] “70’s.” [Online]. Available: http://cr.middlebury.edu/es/altenergylife/70’s.htm.

[10] “What’s the difference between a Li-ion and solid-state battery?” [Online]. Available: https://www.androidauthority.com/lithium-ion-vs-solid-state-battery-726142/.

[11] “The battery technology that could put an end to battery fires - Android Authority.” [Online]. Available: https://www.androidauthority.com/solid-state-battery-technology-723936/.

[12] N. E. Dowling, *Mechanical Behavior of Materials by*, 4th Intern. Pearson, 2013.

[13] B. Barlas, D. Massinon, P. Meyer, G. Cailletaud, I. Guillot, and G. Morin, “A Phenomenological Model for Fatigue Life Prediction of Highly Loaded Cylinder Heads,” 2006.

[14] M. Garat and G. Laslaz, “Improved Aluminium Alloys for Common Rail Diesel Cylinder Heads,” *Trans. Am. Foundry Soc.*, vol. 115, no. 07-, pp. 1–8, 2007.

[15] D. Crolla, *Encyclopedia of Automotive Engineering*. Chichester, UK: John Wiley & Sons, Ltd, 2014.

[16] Halászi Csaba, G. Christian, and D. Helmut, “Fatigue Life Prediction of Thermo-machanically Loaded Engine Components,” in *11th European Automotive Congress, EAEC 2007, Budapest, Hungary*, 2007, pp. 1–14.

[17] E. Charkaluk, A. Bignonnet, A. Constantinescu, and K. Dang Van, “Fatigue design of

structures under thermomechanical loadings," *Fatigue Fract. Eng. Mater. Struct.*, vol. 25, no. 12, pp. 1199–1206, 2002.

[18] T. Takahashi, A. Koike, and K. Sasaki, "Inelastic Behavior and Low Cycle Fatigue of Aluminum Alloy Subjected to Thermo-Mechanical Loading," 1998.

[19] J. J. Thomas, L. Verger, A. Bignonnet, and E. Charkaluk, "Thermomechanical design in the automotive industry," *Fatigue Fract. Eng. Mater. Struct.*, vol. 27, no. 10, pp. 887–895, 2004.

[20] M. Vogler, "The Effect of Pre-Deformation on Ageing Behaviour of Aluminium Alloy A356.0-T7," Chalmers University, 2016.

[21] Tsuyoshi-Takahashi and K. Sasaki, "Low cycle thermal fatigue of aluminum alloy cylinder head in consideration of changing metrology microstructure," in *Procedia Engineering*, 2010, vol. 2, no. 1, pp. 767–776.

[22] D. Ovono Ovono, I. Guillot, and D. Massinon, "Study on low-cycle fatigue behaviours of the aluminium cast alloys," *J. Alloys Compd.*, vol. 452, no. 2, pp. 425–431, 2008.

[23] R. Minichmayr, M. Riedler, G. Winter, H. Leitner, and W. Eichlseder, "Thermo-mechanical fatigue life assessment of aluminium components using the damage rate model of Sehitoglu," *Int. J. Fatigue*, vol. 30, no. 2, pp. 298–304, 2008.

[24] S. Tabibian, E. Charkaluk, A. Constantinescu, F. Szmytka, and A. Oudin, "TMF-LCF life assessment of a Lost Foam Casting A319 aluminum alloy," *Int. J. Fatigue*, vol. 53, pp. 75–81, 2013.

[25] E. Charkaluk and A. Constantinescu, "An energetic approach in thermomechanical fatigue for silicon molybdenum cast iron," *Mater. High Temp.*, vol. 17, no. 3, pp. 373–380, Aug. 2000.

[26] J. P. Sermage, J. Lemaitre, and R. Desmorat, "Multiaxial creep-fatigue under anisothermal conditions," *Fatigue Fract. Eng. Mater. Struct.*, vol. 23, no. 3, pp. 241–252, 2000.

[27] S. Tabibian, E. Charkaluk, A. Constantinescu, A. Oudin, and F. Szmytka, "Behavior, damage and fatigue life assessment of lost foam casting aluminum alloys under thermo-mechanical fatigue conditions," in *Procedia Engineering*, 2010, vol. 2, no. 1, pp. 1145–1154.

[28] K. N. Smith, P. Watson, and T. H. Topper, "Stress-Strain Function for the Fatigue of Metals," *Journal of Materials*, vol. 5. pp. 767–778, 1970.

[29] J. Morrow, "Cyclic Plastic Strain Energy and Fatigue of Metals," in *Internal Friction, Damping, and Cyclic Plasticity*, 100 Barr Harbor Drive, PO Box C700, West Conshohocken, PA 19428-2959: ASTM International, pp. 45-45–43.

[30] C. E. Feltner and J. D. Morrow, "Microplastic Strain Hysteresis Energy as a Criterion for Fatigue Fracture," *J. Basic Eng.*, vol. 83, no. 1, p. 15, 1961.

[31] P. P. Benham and H. Ford, "Low Endurance Fatigue of a Mild Steel and an Aluminium Alloy," *J. Mech. Eng. Sci.*, vol. 3, no. 2, pp. 119–132, Jun. 1961.

[32] William D. Jr. Callister, *Materials Science and Engineering: An Introduction*, 7th ed. Wiley Publishers, 2006.

[33] C. H. Cáceres, I. L. Svensson, and J. A. Taylor, “Strength-ductility behaviour of Al-Si-Cu-Mg casting alloys in T6 temper,” *Int. J. Cast Met. Res.*, vol. 15, no. 5, pp. 531–543, 2003.

[34] T. Bogdanoff, S. Seifeddine, and A. Dahle, “The effect of SI content on microstructure and mechanical properties of Al-Si alloy,” *La Metall. Ital.*, vol. 108, no. 6, 2016.

[35] C. H. Cáceres, T. Din, A. K. M. B. Rashid, and J. Campbell, “Effect of aging on quality index of an Al-Cu casting alloy,” *Mater. Sci. Technol.*, vol. 15, no. 6, pp. 711–716, 1999.

[36] R. E. Stoltz and R. M. Pelloux, “The Bauschinger effect in precipitation strengthened aluminum alloys,” *Metall. Trans. A*, vol. 7, no. 8, pp. 1295–1306, 1976.

[37] M. Zhu, Z. Jian, G. Yang, and Y. Zhou, “Effects of T6 heat treatment on the microstructure, tensile properties, and fracture behavior of the modified A356 alloys,” *Mater. Des.*, vol. 36, pp. 243–249, 2012.

[38] G. A. Edwards, K. Stiller, G. L. Dunlop, and M. J. Couper, “The composition of fine-scale precipitates in Al-Mg-Si alloys,” *Mater. Sci. Forum*, vol. 217–222, pp. 713–718, 1996.

[39] P. Ouellet, F. H. Samuel, D. Gloria, and S. Valtierra, “Effect of Mg content on the dimensional stability and tensile properties of heat treated Al-Si-Cu (319) type alloys,” *Int. J. Cast Met. Res.*, vol. 10, no. 2, pp. 67–78, 1997.

[40] J. A. Taylor, G. B. Schaffer, and D. H. StJohn, “The role of iron in the formation of porosity in Al-Si-Cu-based casting alloys: Part I. Initial experimental observations,” *Metall. Mater. Trans. A Phys. Metall. Mater. Sci.*, vol. 30, no. 6, pp. 1643–1650, 1999.

[41] J. A. Taylor, G. B. Schaffer, and D. H. StJohn, “The role of iron in the formation of porosity in Al-Si-Cu-Based casting alloys: Part II. A phase-diagram approach,” *Metall. Mater. Trans. A Phys. Metall. Mater. Sci.*, vol. 30, no. 6, pp. 1651–1655, 1999.

[42] J. A. Taylor, G. B. Schaffer, and D. H. Stjohn, “The role of iron in the formation of porosity in Al-Si-Cu-based casting alloys: Part III. A microstructural model,” *Metall. Mater. Trans. A Phys. Metall. Mater. Sci.*, vol. 30, no. 6, pp. 1657–1662, 1999.

[43] H. ; Iwahori,Hiroaki ; Takamiya, K. ; Yonekura, Y. Yamamoto, and M. ; Nakamura, “Influence of Iron and Manganese on Feedability of AC2B Aluminum Alloy,” *Im.*, vol. 60, no. 9, pp. 590–595, 1988.

[44] L. Ceschini, A. Morri, A. Morri, A. Gamberini, and S. Messieri, “Correlation between ultimate tensile strength and solidification microstructure for the sand cast A357 aluminium alloy,” *Mater. Des.*, vol. 30, no. 10, pp. 4525–4531, 2009.

[45] S. Thompson, S. L. Cockcroft, and M. a. Wells, “Advanced light metals casting development: solidification of aluminium alloy A356,” *Mater. Sci. Technol.*, vol. 20, no. February, pp. 194–200, 2004.

[46] E. Carrera, J. Alejandro González, J. Talamantes-Silva, and R. Colás, “Effect of the delay in time between cooling and aging in heat-treated cast aluminum alloys,” *Metall. Mater. Trans. B Process Metall. Mater. Process. Sci.*, vol. 42, no. 5, pp. 1023–1030, 2011.

[47] M. Zamani, S. Seifeddine, and E. Ghassemali, “Effect of cooling rate and eutectic

modification on texture and grain structure of Al-Si-Cu-Mg die cast alloy," *Metall. Ital.*, vol. 108, no. 6, pp. 5–8, 2016.

[48] S. Seifeddine, E. Sjölander, and T. Bogdanoff, "On the Role of Copper and Cooling Rates on the Microstructure, Defect Formations and Mechanical Properties of Al-Si-Mg Alloys," *Mater. Sci. Appl.*, vol. 04, no. 03, pp. 171–178, 2013.

[49] E. Sjölander and S. Seifeddine, "The heat treatment of Al-Si-Cu-Mg casting alloys," *Journal of Materials Processing Technology*, vol. 210, no. 10. pp. 1249–1259, 2010.

[50] E. Sjölander, S. Seifeddine, and F. Fracasso, "Influence of Quench Rate on the Artificial Ageing Response of an Al-8Si-0.4Mg Cast Alloy," *Mater. Sci. Forum*, vol. 828–829, pp. 219–225, 2015.

[51] B. Zhang, M. Garro, M. Leghissa, A. Giglio, and C. Tagliano, "Effect of Dendrite Arm Spacing on Mechanical Properties of Aluminum Alloy Cylinder Heads and Engine Blocks," 2005.

[52] M. Zamani, S. Seifeddine, and A. E. W. Jarfors, "High temperature tensile deformation behavior and failure mechanisms of an Al–Si–Cu–Mg cast alloy — The microstructural scale effect," *Mater. Des.*, vol. 86, pp. 361–370, 2015.

[53] E. Merhy, L. Rémy, H. Maitournam, and L. Augustins, "Crack growth characterisation of A356-T7 aluminum alloy under thermo-mechanical fatigue loading," *Eng. Fract. Mech.*, vol. 110, pp. 99–112, Sep. 2013.

[54] R. Fuoco and M. Moreira, "Fatigue cracks in aluminum cylinder heads for diesel engines," *Int. J. Met.*, vol. 4, no. 4, pp. 19–32, 2010.

[55] I. Koutiri, D. Bellett, F. Morel, L. Augustins, and J. Adrien, "High cycle fatigue damage mechanisms in cast aluminium subject to complex loads," *Int. J. Fatigue*, vol. 47, pp. 44–57, 2013.

[56] I. Koutiri, D. Bellett, F. Morel, and E. Pessard, "A probabilistic model for the high cycle fatigue behaviour of cast aluminium alloys subject to complex loads," *Int. J. Fatigue*, vol. 47, pp. 137–147, 2013.

[57] "ASTM E1251-17a, Standard Test Method for Analysis of Aluminum and Aluminum Alloys by Spark Atomic Emission Spectrometry," *ASTM Int.*, 2017.

[58] D-Lab, "Metal analysis." [Online]. Available: http://www.degerforslab.se/en-us/Services/Metal-Analyses#al.

[59] S. Tabibian, E. Charkaluk, A. Constantinescu, F. Szmytka, and A. Oudin, "TMF criteria for Lost Foam Casting aluminum alloys," *Fatigue Fract. Eng. Mater. Struct.*, vol. 36, no. 4, pp. 349–360, 2013.

[60] Astm, "E8/E8M standard test methods for tension testing of metallic materials 1," *Annu. B. ASTM Stand. 4*, vol. i, pp. 1–27, 2010.

[61] ASTM, "ASTM E606/E606M - 12: Standard Test Method for Strain-Controlled Fatigue Testing," *ASTM Standards*, 2012. [Online]. Available: http://www.astm.org/cgi-bin/resolver.cgi?E606E606M.

[62] "Instron : Materials Testing Machines for Tensile, Fatigue, Impact, Rheology and Structural Testing - Instron." [Online]. Available: http://www.instron.us/en-us.

[63] L. Y. Zhang, Y. H. Jiang, Z. Ma, S. F. Shan, Y. Z. Jia, C. Z. Fan, and W. K. Wang, “Effect of cooling rate on solidified microstructure and mechanical properties of aluminium-A356 alloy,” *J. Mater. Process. Technol.*, vol. 207, no. 1–3, pp. 107–111, Oct. 2008.

[64] S. Tabibian, E. Charkaluk, A. Constantinescu, G. Guillemot, and F. Szmytka, “Influence of process-induced microstructure on hardness of two Al-Si alloys,” *Mater. Sci. Eng. A*, vol. 646, pp. 190–200, 2015.

[65] Q. G. Wang and C. H. Caceres, “On the strain hardening behaviour of Al-Si-Mg casting alloys,” *Mater. Sci. Eng. A*, vol. 236, pp. 106–109, 1997.

[66] M. Azadi and M. M. Shirazabad, “Heat treatment effect on thermo-mechanical fatigue and low cycle fatigue behaviors of A356.0 aluminum alloy,” *Mater. Des.*, vol. 45, pp. 279–285, 2013.

[67] Q. G. Wang, “Microstructural effects on the tensile and fracture behavior of aluminum casting alloys A356/357,” *Metall. Mater. Trans. A*, vol. 34, no. 12, pp. 2887–2899, Dec. 2003.

[68] W. H. Hunt, J. R. Brockenbrough, and P. E. Magnusen, “An Al-Si-Mg Composite Model System - Microstructural Effects on Deformation and Damage Evolution,” *Scr. Metall. Mater.*, vol. 25, no. 1, pp. 15–20, 1991.

[69] J. Lemaitre and J.-L. Chaboche, *Mechanics of solid materials*. Cambridge: Cambridge University Press, 1990.

[70] J. Ahlström and B. Karlsson, “Fatigue behaviour of rail steel - A comparison between strain and stress controlled loading,” in *Wear*, 2005, vol. 258, no. 7–8, pp. 1187–1193.

[71] K. U. Snowden, “Dislocation arrangements during cyclic hardening and softening in A1 crystals,” *Acta Metall.*, vol. 11, no. 7, pp. 675–684, 1963.

[72] J. C. Grosskreutz, “The mechanisms of metal fatigue (I),” *Phys. Status Solidi*, vol. 47, no. 1, pp. 11–31, Sep. 1971.

[73] K. (Chalmers U. Runesson, *Constitutive modeling of engineering materials – Theory and computation*, 7th ed. Göteborg, 2005.

[74] Dassault Systèmes Simulia, “Abaqus Documentation.” Dassault Systèmes Simulia Corp, Providence, RI, USA, 2014.

[75] L. Coffin, “A study of the effects of cyclic thermal stress on a ductile metal,” *Trans. Am. Soc. Mech. Eng.*, vol. 76, pp. 931–950, 1954.

[76] S. S. Manson, “Behavior of Materials Under Conditions of Thermal Stress,” *NACA Tech. Note*, vol. 2933, 1953.

[77] B. Zhang, J. Liu, S. Zhang, S. Zhang, and X. Hu, “Tensile ductility improvement of AlSi9Cu1 alloy by chemical composition optimization,” *China Foundry*, vol. 14, no. 2, pp. 80–84, Mar. 2017.

[78] M. B. Grieb, H. J. Christ, and B. Plege, “Thermomechanical fatigue of cast aluminium alloys for cylinder head applicationsexperimental characterization and life prediction,” in *Procedia Engineering*, 2010, vol. 2, no. 1, pp. 1767–1776.